Building a Strontium Clock Laser

Florian Vogl

Masterthesis

submitted
to the faculty of

Mathematics, Computer Science, and Physics

of the University of Innsbruck

Supervisors:

Dr. Florian Schreck
Dr. Rudolf Grimm

11th April, 2013

Contents

1 Introduction **1**

2 Theoretical overview **4**
2.1 Diode lasers 5
2.2 Laser stability 7
2.3 Laser linewidth 9
2.4 Laser noise 11
2.5 The Pound-Drever-Hall stabilization scheme 14
2.6 Resonators 21
2.6.1 The plane-mirror resonator 21
2.6.2 Measuring the finesse 25
2.6.3 The spherical-mirror resonator 27
2.6.4 The modes of the spherical mirror resonator 28
2.6.5 The instability of asymmetric mirror resonators near the confocal configuration 30

3 Experimental setup and results **34**
3.1 Two-stage stabilization setup 35
3.2 Overview over the setup 37
3.3 The Toptica DL 100 pro 39
3.4 Fiber coupling and beam shaping 40
3.4.1 Finding the right polarization angle for coupling . . . 40
3.4.2 Beam shaping 41
3.5 kHz-cavity 42
3.5.1 Experimental details of the kHz-cavity 42
3.5.2 Assembly instructions for the kHz-cavity 48
3.5.3 Experimental results for the kHz-cavity 49
3.6 Estimation of the linewidth after the kHz-lock 54
3.7 Hz-cavity 55
3.7.1 Experimental details of the Hz-cavity 55
3.7.2 Assembly instructions for the Hz-cavity 59
3.8 Electro-optic modulator 62
3.8.1 Experimental details for the electro-optic modulator . 62

3.8.2 Assembly instructions for the electro-optic modulator . 65
3.8.3 Suggestions for improving the electro-optic modulator 65
3.9 Assembling the LC circuit for the electro-optic modulator . . 66
3.9.1 Step-by-step instructions for assembling the LC circuit 66
3.10 Vibration isolation system and breadboards 71
3.11 Fiber stabilization 73

4 Current status of the project and outlook 74

Chapter 1

Introduction

In today's modern society lasers of every kind are truly ubiquitous. Since its invention in the 1960s lasers have found their way into various indispensable roles in research, industry, communications, military, and medicine. To satisfy the needs of all these applications, lasers with different properties are required.

Apart from the laser's intrinsic qualities of high luminance, monochromaticity, directionality, and coherence, certain applications may demand a certain wavelength, intensity or frequency stability.

As no laser is suited for all applications, there has been considerable effort to develop and invent new laser types and technologies. Nowadays, there are many different types of lasers (gas lasers, dye-lasers, diode lasers, quasi-molecular lasers etc.) and technologies (laser modulation techniques, Q-modulation, amplifying technology, frequency stabilizing techniques, nonlinear technology etc.) that can be applied to match the need of a certain application as closely as possible [1].

The field of quantum physics is very intricately linked to the progress in laser technology. Many breakthroughs in the different fields of quantum physics would have been impossible without certain advancements in laser technology. One very famous of example of this fact is the invention of laser cooling and trapping techniques in the 1980s, for which Steven Chu, Claude Cohen-Tannoudji, and William D. Phillips were awarded the nobel price in 1997.

As quantum physics very often involves light-matter interactions of some sort, the high flexibility of and high control one can gain over lasers makes them indispensable tools in most quantum physic laboratories.

The world of quantum physics and precision measurements deal with very delicate systems, so lasers in these research fields often face the most challenging requirement in terms of frequency stability, intensity stability, absolute wavelength controllability, as well as directionality and mode properties. Thought there have been many advancements in lasers in the last years, a very significant one has certainly been the progress towards ultrastable lasers with extraordinary frequency stability and frequency accuracy.

With fractional frequency stabilities on the order of 10^{-16} [2, 3], these lasers can be used for a multitude of high precision experiments. Optical clocks based on these ultrastable lasers have recently achieved a fractional inaccuracy of $8.6 \cdot 10^{-18}$ [4] and instabilities of $\sigma_y = 4...5 \cdot 10^{-16}/\sqrt{\tau/s}$ [2], making them presently the most precise measurement devices for time and frequency [5].

Ultrastable lasers are indispensable tools in experiments to measure gravitational waves (LIGO project etc.) or in experiments to measure possible changes in fundamental physical constants [6]. Furthermore ultrastable lasers allow the efficient coupling to quantum states with exceptionally long lifetime, which allows for interesting applications in quantum computation [7] and quantum simulation[8]. An review over many of the experiments, possi-

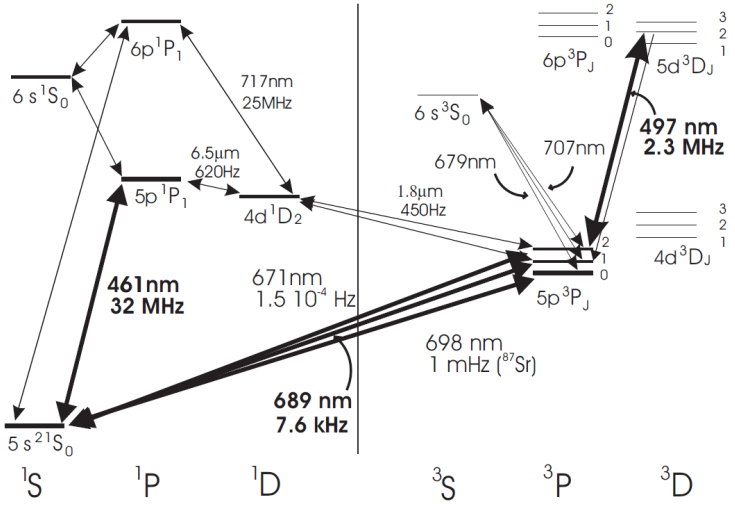

Figure 1.1: Schematic of some states and transitions of Strontium. The clocklaser presented in this work will work on the 5^1S_0 and 5^3P_0-transition with a wavelength of 698 nm. Figure taken from [10].

ble with Strontium and ultastable lasers on its clock transitions (prominently $5^1S_0 - 5^3P_0$), can be found in reference [9].

After we have now presented some of the many possibilities such a laser system can offer to quantum experiments, this work will continue with describing the progress made towards building an ultrastable laser with a linewidth of 10 Hz or better for the rubidium-Strontium experiment of Florian Schreck at the Institute for Quantum Optics and Quantum Information in Innsbruck, Austria.

The absolute wavelength of the laser is 698 nm and will be used to couple the 5^1S_0 and 5^3P_0-states of Strontium (see Fig. 1.1) for various applications, some of which are discussed in Sec 4 as the nearest applications for the laser. Other groups around the globe have built similar projects [11–14], which might offer additional information to the interested reader.

This master thesis is divided into an introduction, a theoretical and an experimental chapter and an outlook. Chapter 2 introduces the physical concepts and basic theories relevant for understanding the setup and intricacies involved and chapter 3 discusses the setup itself and presents experimental measurements and assembly instructions for the setup. Chapter 4 summarizes the current status of the project and gives a short outlook on the possible applications of this ultrastable laser in the near future.

Chapter 2

Theoretical overview

This section presents an overview over the principles involved in laser stabilization. Specifically we will focus on our application of stabilizing a diode laser by using an interference-based approach, the Pound-Drever-Hall scheme [15] [16]. For the reader that is not yet familiar with the basics of laser theory we recommend references [17] as an introduction, [18] and [19] for all-round information and [20] for a theoretical discussion.

2.1 Diode lasers

Diode lasers have become indispensable tools in the laboratory over the years. They are compact, robust, cheap, maintenance-free and available at plenty of wavelengths. While other laser systems may still be the better choice, when special properties like the immense tunability of a Titan:sapphire laser or the power of a CO_2 laser are needed, many jobs can nowadays be done by diode lasers. For more extensive information on diode lasers, see for example references [21] and [18].

A diode laser uses a crystal of a semiconductor like GaAlAs as a gain medium. As shown in figure 2.1 a n-doped region and a p-doped region are created through doping of the crystal[1]. The doping changes the usual band structure of the semi-conductor slightly[2], because the dopants are of a different element than the crystal itself.

As shown in figure 2.1, in the n-doped region, where electrons are abundant because the layer got doped with an atom sort of a chemical group higher than the crystal species (thus having one more electron in its outmost shell), additional energy levels appear right beneath the edge of the conduction band. In the p-doped zone, where electrons are rare and therefor the quasi-particle holes are abundant, additional energy levels appear energetically right above the valence band. When a current (the injection current) is driven through the crystal in forward direction, electrons travel in the additional levels right beneath the conduction band of the n-doped layer towards the p-doped region. There they can not continue, as there are no levels of equal energy in the p-doped region, and consequently fall down to the vacant, additional energy levels above the valence band in the p-region.

As this process can be seen as electrons coming from the n-doped region and holes coming from the p-doped region, recombining in the active region, one speaks of electron-hole recombination. The energy difference ΔE between the two involved energy levels is emitted in form of a photon with energy $\Delta E = h\nu$, where h is Planck's constant and ν is the light's frequency. This relation means that the laser's wavelength is dominantly determined

[1] We are assuming the most straight forward case of a single active layer here. While there are different designs, for example to achieve extraordinary high powers by using multiple active layers, the basic principle does not change.

[2] For an explanation, why arranging atoms (that have very sharp energy levels) in a crystal lattice leads to energy bands, see [22] and [23]

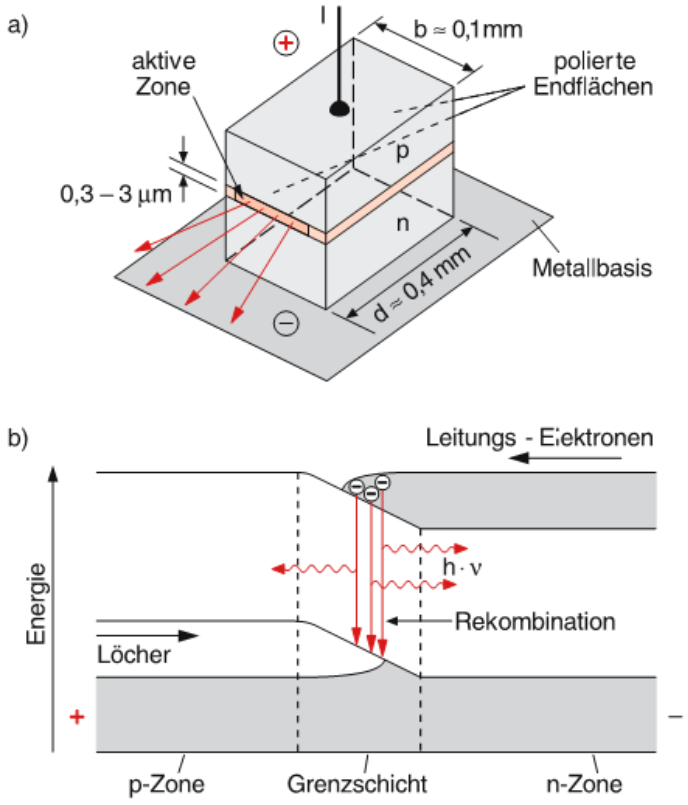

Figure 2.1: Top: A semiconductor is divided into a p-doped region and a n-doped region. When an injection current is applied, electrons from the n-doped region recombine in the active layer with the holes from the p-doped region, emitting photons in the process. The cleaved facets of the crystal act as mirrors of a laser resonator through the change in refractive index from crystal to air. Bottom: Energy-level structure of the diode laser. The usual band structure of the semiconductor, consisting of the conduction band (higher energy) and valence band (lower energy) is modified by the doping. In the n-doped region additional energy levels appear right beneath the conduction band, while in the p-region additional energy levels right above the valence band are created. Image taken from [19] with kind permission of Springer Science+Business Media.

by the the band-gap of the used semi-conductor, while the linewidth of the emitted light is usually much bigger than the linewidth of the atoms' spectral widths involved, because of the energy spreads in the additional levels created by the doping[3].

[3] In a very simplified picture one could imagine an electron from an energy level right at the bottom of the valence band (the additional level with the highest energy) recombining

The selection of the transverse mode of the laser is either accomplished by spatially changing the index of refraction or by a spatially varying injection current density, for more information see reference [18].

Usually the cleaved surfaces of the crystal itself act as mirrors of a laser resonator, due to the reflection arising at the change of refractive index between the crystal and air. If a different finesse is needed for the resonator, the surfaces can be reflection coated to give higher reflectivity or the output surface can be anti-reflection coated to decrease the finesse of the resonator.

While diode lasers usually have an output power in the range of $10 - 20\,\mathrm{mW}$, coatings alone can push this value to $50\,\mathrm{mW}$. Still higher powers are often possible but need more sophisticated approaches.

The output power and the wavelength of a diode laser can be controlled by varying the induction current or the diode's temperature. This is because the current density and temperature both change the refractive index of the material, changing the length of the laser resonator. As a resonator only allows standing waves with a wavelength satisfying the relation $L = n\lambda/2$, where L is the effective length of the resonator, n is an integer and λ is the wavelength of the light, this shifts the maximum gain of the resonator to another wavelength, changing the emitted wavelength of the laser. For more information on resonators see Sec. 2.6.

2.2 Laser stability

Even though many people speak about frequency stability of a laser as if this was an unambiguous, clearly defined term, we will see that there are different kinds of frequency stability and one has to make clear which one is meant.

First one has to be aware that **every measurement** is uncertain to some extent. For example our methods and devices could give a value slightly off the real value of the quantity (in our case the frequency) we want to measure. Or we could get values that vary slightly when measured multiple times.

This is why there are specific concepts in the scientific methods to quantify the properties of the measurement methods used. Examples for these basic concepts are accuracy, precision, repeatability and reproducibility.

In this work we will only present some concepts used in the field of laser stabilization, which have actually been inspired by the above, basic concepts. Because of this they naturally have some similarity but we want to emphasize that the basic concepts apply to **every measurement** while

with a hole from a level at the bottom OR the top of the additional levels in the p-doped region. This would lead to an energy difference according to the difference in energy between the lowest and highest energy level of the p-doped additional energy levels, which would consecutively lead to a frequency difference of the emitted photons for the two processes.

terms like frequency stability and frequency reproducibility, are quantities **derived** from such measurements.

When people talk about laser stability, they usually are talking about the ratio of the frequency variation $\Delta\nu$ to the average frequency $\overline{\nu}$ in a **certain timeframe** τ. In this work we define the frequency stability [1] by

$$S_\nu(\tau) = \frac{\Delta\nu(\tau)}{\overline{\nu}}. \tag{2.1}$$

The smaller the amount of variation in the frequency over the timeframe, the smaller S and the better the frequency stability[4]. While using the root-mean-square of the signal for $\Delta\nu$ gives a dimensionless quantity, more often people prefer to work with the variance as $\Delta\nu$, which leads to the stability S having the units of $\mathrm{Hz}/\sqrt{\mathrm{Hz}}$.

This definition involves some subtleties, so we want to point out some things to be aware of when working with this quantity. Notice how the stability S is defined as a ratio of measurable quantities. This means that the same variation of 1 kHz in the chosen timeframe can lead to totally different stabilities, depending on the average frequency emitted by the source. So one always has to keep in mind, which kind of source one is dealing with – is it a laser emitting visible light with a frequency of around 10^{14} Hz or a microwave source emitting radiation with a frequency of some hundred MHz – to make any statements about the absolute quantities, like the frequency variation, possible. Next it is of utmost importance to give the **timeframe** τ in which the quantities were measured, when talking about stability. When choosing small enough timeframes, every system will be very stable, as it has not had time enough to change its frequency significantly (this of course means choosing τ smaller than any other typical timescale of the system).

For the laser to be usable in high-precision experiments it is important that it not only has a **good stability** (meaning low values of S) but also has high **frequency reproducibility**. The idea behind this is, that while the laser source should be stable at a certain frequency, this frequency should be up to standard compared to other systems. It is not only sufficient for a clock, that every second is equally long and thus stable, but a second should also be equally long as every other second somewhere else.

The frequency reproducibility is generally defined as

$$R_\nu(\tau) = \frac{\delta\nu(\tau)}{\overline{\nu}}, \tag{2.2}$$

where $\overline{\nu}$ is again the average frequency over the timeframe τ and $\delta\nu$ is the variation from the stabilized value during the timeframe τ [1].

[4] Often the reciprocal definition $S_\nu(\tau) = \frac{\overline{\nu}}{\Delta\nu(\tau)}$ is chosen as the frequency stability, because this quantity gets bigger when the stability gets better. While this makes sense, it is customary to give the stability in terms of S, like for example $10^{-12}(\tau = 3\,\mathrm{s})$, so we decided to present the more practical definition here.

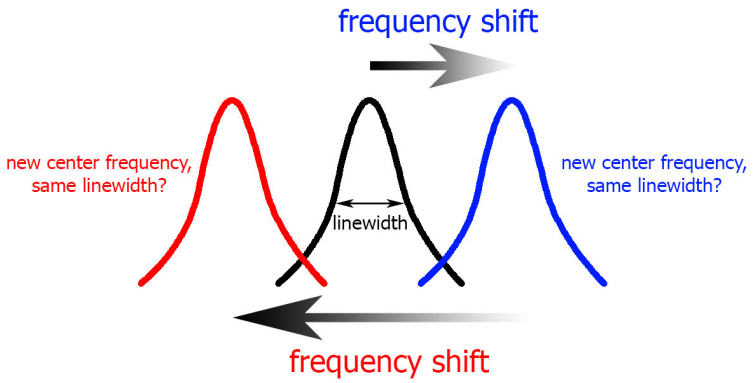

Figure 2.2: Consider a laser, running at a given central frequency with a given linewidth. Now assume we send this laser through a time-dependant shifting device, like an acousto-optic-modulator. Wouldn't this just leave us with a laser with the same linewidth but changing central frequency?

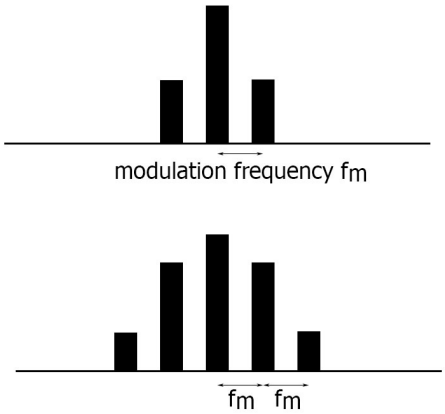

Figure 2.3: Schematic of the resulting spectrum of a laser frequency modulated by a fixed frequency f_m. Depending on the modulation index β (see sections 2.3 and 2.5) the first order sidebands (top, $\beta \approx 1$) are dominant, while sidebands of higher order can get significant at higher modulation index (bottom). At really high modulation indices the carrier disappears, the power being distributed completely to the sidebands.

2.3 Laser linewidth

Strictly speaking, the laser linewidth is the frequency spread around the significant frequency-component peak in the spectrum of the laser's emitted

light. Definitions on how this width is to be calculated vary from full-width-half-maximum of the peak to the width where the waveform falls to $1/e^2$ of its peak value. This section discusses why the term linewidth usually does not refer to this definition and what actually is meant. After this, we discuss how a time-dependant shift in the laser's frequency leads to a change in its linewidth.

Time and frequency domains are related to each other by a Fourier transform

$$f(\omega) = \frac{1}{2}\int_{-\infty}^{\infty} dt f(t) \exp\left(-i\omega t\right), \tag{2.3}$$

where i is the imaginary unit, t is time, $f(t)$ is the waveform with respect to time and $f(\omega)$ is the waveform in terms of frequency.

This definition has the advantage, that by knowing the waveform at **all times** you can determine the frequency components of the oscillation and by knowing the frequency components you can predict the waveform at all times.

But this relation also means, that when talking about the frequency spectrum of a signal, you have to know the waveform at all times – If you only know the waveform for a certain time (say, 2 seconds) you can not know if it changes before or after that, which would alter the resulting spectrum heavily.

Of course relation 2.3 also implied that you can work in the time domain or the frequency domain but **not both at the same time**. So speaking about a "laser with a linewidth of 300 kHz, drifting by $2kHz/s$ due to external influences" strictly speaking does not make sense, as one has to know the behaviour of the laser at **all times** to get the linewidth.

What is actually meant is the following: As measuring a waveform forever tends to get quite boring in practice, people only use a certain time interval τ_0 to determine the spectrum of the light and thus the linewidth.

Formally one determines the spectrum of the light as

$$f(\omega) = \frac{1}{2}\int_{0}^{\tau_0} dt f(t) \exp\left(-i\omega t\right), \tag{2.4}$$

However, by determining the linewidth one introduces an additional timescale τ_0, which has to be appropriate for the system and application to make sense.

At timescales longer than τ_0 one then uses a time-domain approach, while behaviour on timescales shorter than τ_0 are included in the linewidth/spectrum. As both of these definitions are quite different, one should make clear which one is used. Sadly this rarely happens and one has to infer from the context which definition is meant.

In our experimental setup we plan to use an acoustu-optic-modulator (AOM) as an actuator for one of the stabilization loops (see Sec 3.1 for details). Usually an AOM is used to shift the laser's frequency by a certain

amount, depending on the frequency of the radiofrequency signal applied to the AOM. For example one could shift the laser light's frequency by 80 MHz by sending it through an AOM and applying a 80 MHz voltage signal of appropriate strength to the AOM. As the AOM acts as an actuator in the feedback loop, the signal to the AOM will vary in time and thus the laser's frequency will be shifted in varying amounts. The question is now how this process can actually decrease the laser's linewidth, which is the goal of the stabilization scheme. If we send a laser with a linewidth of 300 kHz through the controlled AOM, wouldn't we be just left with a 300 kHz linewidth shifted in center frequency by varying amounts, thus not decreasing the linewidth at all (see figure 2.2)?

The answer is again in the definition of linewidth and in remembering what kind of quantity one is dealing with. One can not speak about sending a laser with a **linewidth** of 300 kHz through an AOM with **time-dependant** behaviour (throught the control-loop). While the laser might have a linewidth of 300 kHz without the AOM, the time-dependant AOM will certainly change the behaviour of the laser **in time**. And after we measured the resulting waveform for some time, we most certainly have a new linewidth. which can be determined by Eqn. 2.4!

We will see another example for this in Sec 2.5, where the light is getting phase modulated by an electo-optic-modulator (EOM) with a fixed frequency. As this is also a time-dependant process, this also changes the spectrum of the radiation, creating sidebands at distances of the modulation frequency, see figure 2.3.

The bottom line is that one has to be aware of the fact that every time-dependant process can change the spectrum of the laser and thus the linewidth of the laser, while details depend on the process in question and the exact definition of linewidth used.

2.4 Laser noise

In this section we present some of the more important noise sources without claiming completeness. We will also focus mainly on noise relevant for a diode laser.

What effects actually determine a laser's linewidth? While many of the dominant effects are of technical nature and can be found and removed rather efficiently, one is still left with a noise floor made up from a multitude of little perturbations. Essentially every perturbation that can change the emitted wavelength of the light in some time-dependant way will contribute to the linewidth, as discussed in Sec 2.3.

The wavelength of emitted light is predominately determined by the atomic transition involved in the laser process as well as the transmission maximum of the laser resonator/cavity (see Sec 2.6 for more details on res-

onators). In case of the diode laser the role of the atomic transition is played by the band gap between the valence band and the conduction band in the semiconductor. As there are many levels involved in the working of a diode laser and because those energy levels can have significant energy spread (see Sec 2.1) the natural width of this transition is usually orders of magnitude higher than the natural linewidth of an atomic transition.

If one assumes that the linewidth $\Delta\nu_t$ of the atomic transition/semiconductor transition is much bigger than the width $\Delta\nu_r$ of the transmission peak of the laser resonator one can determine the emitted radiation's frequency ν from

$$\nu = \nu_r + (\nu_t - \nu_r)\frac{\Delta\nu_r}{\Delta\nu_t}, \tag{2.5}$$

where ν_r is the frequency of the maximum of the laser resonator's transmission peak and ν_t is the frequency of the laser transition (in our case the bandgap) [1]. This relation also means that every time-dependent process, which changes any of the quantities in Eqn. 2.5, will change the frequency of the emitted light and thus change the resulting linewidth.

Because the ratio $\frac{\Delta\nu_r}{\Delta\nu_t}$ is usually very small, the laser's frequency mainly gets determined by the maximum of the resonator's transmission peak. This is also the reason why external cavities work so well to improve wavelength tuning and stability for diode lasers, see for example reference [21].

The resonator's resonance frequencies are given by

$$\nu_t = m\frac{c}{2nL}, \tag{2.6}$$

where m is an integer, c is the speed of light in vacuum, n is the refractive index of the resonator's fill material and L is the length of the resonator (see also Sec 2.6). Differentiating we find that the differential change in resonance frequency $\delta\nu_t$, due to differential changes in refractive index δn or length δL , is

$$|\frac{\delta\nu_t}{\nu_t}| = |\frac{\delta L}{L}| + |\frac{\delta n}{n}|. \tag{2.7}$$

As explain in Sec 2.6 the width Δ_r of the transmission peak of the resonator is dependant on the reflectivity of the resonator's mirrors. The change of this quantity can be neglected, because there usually are no processes that change the reflective of the mirrors in a significant enough way.

We will now list a few of the most significant processes which influence the length and/or refractive index of the cavity, thus potentially affecting the laser's linewidth. If those influences can be minimized, the linewidth can already be decreased significantly without using active stabilization. The same points also apply when one wants to build a stable reference cavity, as will be discussed in the experimental section of this work.

1. Temperature variations lead to a change in the resonator's length through the temperature-expansion coefficient of the filling material and of the mirrors themselves.

   In the case of the diode laser temperature variations affect the semiconductor crystal, which serves as the resonator, and change its length. If the diode laser has an external cavity, temperature changes in the mountings can also lead to a changing cavity length. This is the reason why materials with extraordinarily low temperature-expansion-coefficients are chosen when one is building stable reference cavities (see sections 3.5 and 3.7), so these effects are as small as possible.

   As semiconductors are subject to significant changes in which internal states are occupied depending on temperature (the reason why semiconductors show properties of isolators and conductors, depending on temperature – see [22]), changes in temperature also change the charge carrier density inside the semiconductor. As the charge carrier density is intricately linked to the refractive index n of the material, temperature variations also change the refractive index of the material.

2. Changes in the injection current do influence the emitted frequency in a similar manner to temperature variations. The change in current density changes the refractive index of the material and affects the temperature of the crystal as well, leading to a change in the effective length of the resonator.

3. Vibrations, transmitted through mechanical or acoustical means onto the setup, can change the length of the laser or stabilization scheme resonator, thus changing the emitted wavelength. This can be acoustic noise created by a fan of one of the components nearby or the passage of a vehicle on the road outside the building. To counteract this effect, resonators are often put into vacuum and insulated from vibrations as well as possible. For example, this can be accomplished through the use of optical tables, special mounting geometries and vibration isolation platforms (see also Sec 3.10).

4. Blackbody radiation can lead to heating of the cavity or the mountings. Special care has to be taken when pumps or other electronic devices are mounted near the cavity, as changes in their temperature can be transmitted through changing amounts of blackbody radiation even in vacuum. This effect can be minimized by installing blackbody shields at appropriate places in the setup (see also Sec 3.7).

5. There are some fundamental noise sources, which pose an ultimate limit on the performance of laser stabilization. These include thermomechanical noise of the mirrors and the mirror substrates, due to the Brownian motion at finite temperature [24]. It also includes photon

shot noise, due to the random nature of the photon creation process in lasers [24]. These effects only get important when all the other effects are controlled very well, usually when one wants to push the laser's linewidth to 1 Hz and below. For the most stable lasers in the world, thermo-mechanical noise is the limiting factor at the moment, leading to a search for new materials and techniques to minimize this effect [24].

A more extensive and more detailed discussion of these points can be found in references [24] and [25].

2.5 The Pound-Drever-Hall stabilization scheme

As discussed in the previous sections, every laser is subject to internal and external perturbations, which cause the frequency of the emitted light to change with time. Minimizing the effects discussed in Sec 2.4, for example through vacuum, controlled current sources and temperature stabilization (for more details see the experimental sections), will lead to a more stable system without controlling the lasers's frequency in a direct way. This is why this procedure is known as passive laser stabilization.

Active laser stabilization, on the other hand, measures the frequency of the emitted laser light and **actively** counteracts any disturbances from the frequency, which we want the laser to emit. Basically the effects affecting the laser's frequency, are measured and counteracted by appropriate means, which greatly stabilizes the laser system to the desired frequency.

The idea of measuring a quantity and correcting deviations from a certain set point to stabilize a system is very common in nature. Often given examples include the balance system, that allows us humans to keep upright – our sensory system recognizes when we are about to fall over and corrects this by an appropriate response.

As this concept is very important in biological systems and indispensable in todays technological world, there is a field called control theory, which researches the principles, applications, and possibilities of this (measure–compare to a given value–correct)-feedback loop.

Because control-theory is out of the scope of this work, we refer interested readers to reference [26], which we heavily recommend to every reader not familiar with control theory.

This section will present one of the most successful and widely employed laser stabilization schemes: the Pound-Drever-Hall (PDH) stabilization scheme[5]. The PDH-scheme is the "(compare to a given value)-step" in the steps explained in the preceding paragraph – it creates an error signal,

[5] For other methods to stabilize a laser, see for example chapter 5 in [1].

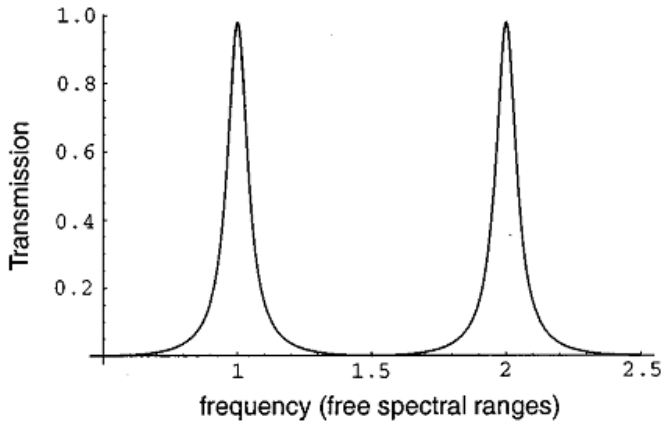

Figure 2.4: Transmission of light through an optical cavity as a function of the light's frequency. The maxima of the peaks are located at multiples of the free spectral range, given by $c/2L$, where c is the speed of light and L the length of the resonator. The lower the reflectivity of the mirrors, the broader the peaks. Figure taken from [27].

quantifying the difference between the actual value of the frequency compared to the setpoint. Much of the information presented in this section is drawn from the excellent paper "An introduction to Pound-Drever-Hall laser frequency stabilization" by E. Black[27].

The basic idea is to transfer the frequency stability of a stable frequency reference onto the frequency stability of the laser. In our case the frequency reference are the transmission lines of a cavity, also called Fabry-Perot interferometer (see also Sec 2.6). In this specific case the goal is to build a highly stable cavity/resonator, which offers very stable transmission peaks at certain resonant frequencies. These transmission peaks can be used as a reference for laser stabilization. To achieve sufficiently stable resonator modes the resonator needs a very stable length and index of refraction, as was discussed in 2.4. Details of optical cavities are also discussed in Sec 2.6.

At this point let us assume that we have managed to successfully build such a cavity and discuss how to transfer the stability from this reference cavity onto the laser's frequency.

Ideally only light with a wavelength of

$$\lambda = \frac{nL}{2}, \tag{2.8}$$

where n is an integer and L is the length of the cavity, gets transmitted

through the cavity. Due to the finite reflectivity of the mirrors the transmission peaks, shown in figure 2.4, have a finite width, depending on the finesse of the cavity. In the limit of perfect mirrors the peaks get infinitely narrow and only light with a wavelength satisfying Eqn. 2.8 gets transmitted.

The goal of the PDH-technique is to choose one of those transmission peaks as a frequency reference and measure deviations from the peak so they can be counteracted (by modulating the laser current in our specific case, see Sec 3.1).

An idea is to measure the intensity transmitted through the cavity and to keep it at a maximum. The problem with this approach is that the form of the transmission peak is symmetric, so a too high frequency leads to a drop in intensity, as does a too low frequency. This makes it impossible for the control system to determine in which direction the laser frequency has to be readjusted. A way to solve this problem is to stabilize not at the maximum but at a point at the flank of the peak. While this works, it suffers from the fundamental problem that one can not distinguish between fluctuations in the laser's intensity and in the laser's frequency. Intensity based approaches to laser stabilization often suffer from this problem (see [1]) and need additional ways to measure or control the intensity to work optimally.

This is why interferometric approaches to laser stabilization are often more advantageous. The PDH-technique is such an interferometric technique and uses phase-modulation to create the sidebands in the frequency spectrum of the carrier (see Fig. 2.3). Because light of different frequencies are influenced differently by the cavity (see Fig. 2.6) the actual wavelength of the carrier can be determined by sending the light onto the cavity and measuring the beat-signal of the sidebands with the carrier.

The PDH-technique also uses the reflected signal from the cavity instead of the transmitted light. By measuring the signal reflected from the cavity, the PDH-technique decouples frequency- from intensity-fluctuations in the laser light, because now we are stabilizing to the point of minimal intensity (instead of the transmission peaks in figure 2.4 we now have transmission-dips). Moreover, using the reflected light makes the response time of the servo-system, the possible bandwidth, independent from the cavity's response time!

The reason for this is that the transmitted light heavily depends on the field inside the cavity, which consists of different contributions from the light's roundtrips inside the cavity (see Sec 2.6). This means that a change in the light's frequency only affects the light transmitted through the cavity after the light has oscillated many times inside the resonator. This delay depends on the cavity's response time, which increases with higher finesse/reflectivities (higher reflectivity means more roundtrips of the light before significant leakage to the transmitted beam). The light reflected from a cavity is actually an interference between the laser light, directly reflected

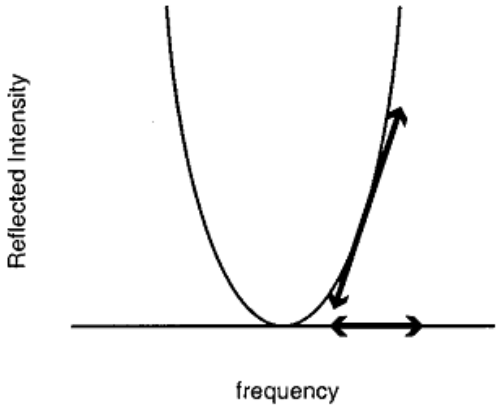

Figure 2.5: A transmission dip in intensity of light reflected of a cavity as a function of the frequency. If you vary the laser frequency and monitor the corresponding change in intensity you can determine whether the frequency is too high or too low compared to the minimum. Figure taken from [27].

at the first mirror, thus not even entering the cavity, and the leakage beam of the field inside the cavity in the backwards direction. As the field inside the the cavity suffers from the delay just discussed, it does not react to a change in the laser light immediately. However, the component reflected at the first mirror does, which means that the total reflected light is influenced by a change in the laser's frequency almost immediately. To be exact, it changes at the same rate as the direct reflection of the mirror is. However, it is not dependant on the cavity's response time!

What basically happens is that the cavity averages the light's frequency over its response time and thereby the leakage beam acts as a stable reference for the component reflected at the first mirror.

As discussed before, we need to create an antisymmetric error-signal, which makes it possible to determine whether the current frequency is too high or too low, compared to the frequency setpoint. The PDH-technique accomplishes this with the help of phase-modulation. The idea behind this is the following: while it is impossible to determine whether the actually frequency is too high or too low compared to the minimum of the reflection dip by measuring the intensity alone, it is possible to infer this information by slightly varying the frequency of the laser and measuring the corresponding change in intensity, see figure 2.5. If the intensity varies in-phase with the frequency modulation (the intensity gets higher when the frequency is increased) the current laser frequency is too high, see also figure 2.6.

This consequently means that by measuring the phase of the reflected

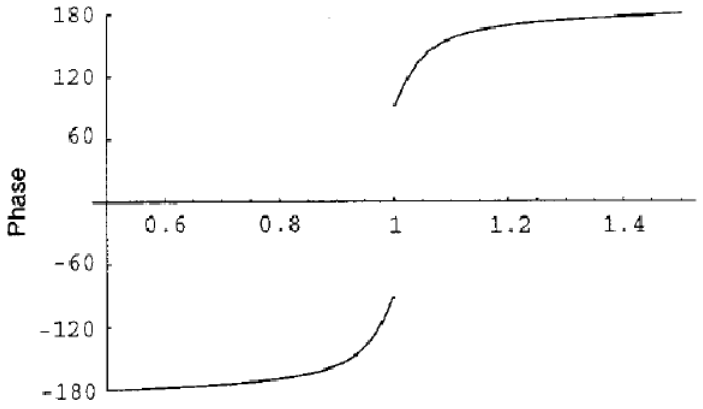

Figure 2.6: Phase shift of a reflected plane wave as a function of frequency. In contrast to the intensity function, the phase function is asymmetric, making it possible to determine whether the frequency is too high or too low compared to the setpoint. Figure taken from [27].

beam, we can determine whether the frequency needs to be in- or decreased to reach resonance (meaning the minimum of the transmission function). Unfortunately there is no measurement device currently available, that is able to measure the electric field's phase directly. According to Glauber's theory of the photodetector, a photodiode only measures the intensity of the light[6]. We now show how the PDH-technique is nevertheless able to determine the phase from the interference between the carrier and the sidebands.

In experimental practice it is more convenient to work with phase- instead of frequency modulation, because phase modulation can be easily achieved through an electo-optic modulator. The phase modulation creates an electric field of the form

$$E_{\text{inc}} = E_0 \exp i(\omega t + \beta \sin \Omega t), \tag{2.9}$$

where ω is the carrier's frequency, E_0 the amplitude of the carrier, Ω is the modulation frequency and β is the modulation index, which is a measure for the strength of modulation [27].

By expanding this expression as a Fourier series and assuming that β is small, we find the dominant terms

$$E_{\text{inc}} \approx E_0 \left[J_0(\beta) \exp i\omega t + J_1(\beta) \exp i(\omega + \Omega)t - J_1(\beta) \exp i(\omega - \Omega)t \right], \tag{2.10}$$

[6] More exactly, one is measuring the quantity $\langle \psi | E_i^{(-)}(x_D, t) E_j^{(+)}(x_D, t) | \psi \rangle$, where i, j are the cartesian components of the electric field, x_D is the position of the detector, t is the time and the minus and plus symbolize the negative or positive frequency part of the complex electric field. See for example R. Glauber, Les Houches Lectures Notes 1964.

where J_x is the Bessel function of the x-th order [24], see also figure 2.3. This means that additionally to the carrier with frequency ω and an amplitude given by $J_0(\beta)$, sidebands with a frequency $\omega+\Omega$ and $\omega-\Omega$ and an amplitude of $J_1(\beta)$ are created. The sidebands have different phase (as have all other odd-sidebands in the expansion) and the fraction of power in the sidebands is determined by the modulation index β. At high enough modulation higher order sidebands have also significant amplitude and have to be included in the considerations. For the PDH-technique it is optimal when the power in each of the first order sidebands is half the power of the carrier [27].

For an ideal cavity the reflection coefficient $F(\omega)$, the ratio between the incoming and reflected light fields, is given by

$$F(\omega) = E_{\text{ref}}/E_{\text{inc}} = \frac{r\left[\exp i\frac{\omega}{\Delta\nu_{\text{fsr}}-1}\right]}{1-r^2\exp i\frac{\omega}{\Delta\nu_{\text{fsr}}}}, \tag{2.11}$$

where $\Delta\nu_{\text{fsr}} = c/2L$ is the free spectral range and r is the reflectivity of the mirrors.

From this expression, one can calculate the reflected electric field by multiplying each component of the incoming electric field (Eqn. 2.10) with the appropriate reflection coefficient

$$\begin{aligned} E_{\text{ref}} = E_0[&F(\omega)J_0(\beta)\exp i\omega t + F(\omega+\Omega)J_1(\beta)\exp i(\omega+\Omega)t \\ &-F(\omega-\Omega)J_1(\beta)\exp i(\omega-\Omega)t]. \end{aligned} \tag{2.12}$$

As the photodetector only measures the intensity, we are interested in the expression $P_{\text{ref}} = \|E_{\text{ref}}\|^2$. The multiplication gives terms from each component with itself as well as the interference terms between the three components. While the square terms are not time dependant, the interference terms oscillate at a frequency of the difference and sum of the frequencies of the components involved. This means that the interference terms between the carrier and a sideband oscillates at the modulation frequency Ω and $2\omega\pm\Omega$. In the end we are left with terms of the form

$$\begin{aligned} P_{\text{ref}} = &\text{ const. terms}+ \\ 2\sqrt{P_cP_s}&\text{Re}\left[F(\omega)F^*(\omega+\Omega) - F^*(\omega)F(\omega-\Omega)\right]\cos\Omega t+ \\ 2\sqrt{P_cP_s}&\text{Im}\left[F(\omega)F^*(\omega+\Omega) - F^*(\omega)F(\omega-\Omega)\right]\sin\Omega t+ \\ &2\ \Omega\text{ terms and terms involving }\omega, \end{aligned} \tag{2.13}$$

where P_c and P_s are the power of the carrier and one sideband component respectively. By adapting the phase shift between the local oscillator and the reflected signal you can make either the sine or cosine term in Eqn. 2.13 average to zero. By filtering out only the remaining term at frequency Ω (for example using a mixer and a lowpass filter, see Sec 3.8.1), the quantity

$$F(\omega)F^*(\omega+\Omega) - F^*(\omega)F(\omega-\Omega) \tag{2.14}$$

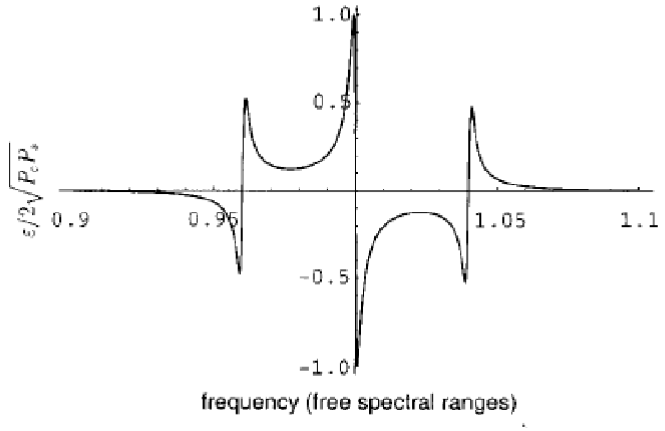

Figure 2.7: The Pound-Drever-Hall error signal as a function of the frequency deviation from the setpoint, when the modulation frequency Ω is high and only the sine term in Eqn. 2.13 survives (constants were omitted). The distance to the sidepeaks is given by the modulation frequency Ω, while the slope of the central peak is mainly determined by the finesse of the cavity and influences the possible performance. Figure taken from [27].

can be measured.

Figure 2.7 shows the resulting PDH error signal as a function of the frequency deviation from the setpoint (in our case a specific reflection dip from the reference cavity), when the modulation frequency Ω is much higher than Δ_{fsr}/F), where F is the finesse of the cavity. In this case only the sine term in Eqn. 2.13 survives. The function is asymmetric, so the sign of the signal tells the control system whether the frequency of the laser needs to be in- or decreased. The sidepeaks are located at a distance Ω from the carrier, which means that the capture range of the lock is determined by the modulation frequency Ω. This means that it is convenient to choose comparably high modulation frequencies, as long as there are no other transmission dips in this range. This would start a new PDH error signal of the form shown in figure 2.7, that has additional zero points, thus decreasing the capture range (see also Sec 3.8.1).

The slope of the main peak zero point crossing is given by

$$-\frac{8\sqrt{P_c P_s}}{\delta\nu}, \tag{2.15}$$

where $\delta\nu = \Delta\nu_{\mathrm{fsr}}/F$ is the cavity's linewidth, determined by the free spectral range ν_{fsr} and the finesse F. As this error signal is linear in the frequency, we can use the standard tools of control theory to stabilize the laser [26].

This slope fundamentally determines how well the lock can perform and how well the laser can be stabilized. To achieve small linewidths one has to use a cavity with a very small cavity linewidth, achievable by a high finesse and small free spectral range.

As the error signal is created by extracting the term oscillating at the modulation frequency Ω from Eqn. 2.13, noise terms at this frequency will influence the error signal in a very strong way. For example amplitude modulation arising at the electro optic modulator, due to coupling to a radiofrequency source or time-dependent parasitic etalon effects inside the crystal, are demodulated together with the error signal and give an offset to the signal. This can lead to problems, because the control system locks to the zero point of the error signal – especially if the residual amplitude modulation drifts with time, so these effects have to be taken care of.

As a more extensive discussion of noise sources and their influence on the stabilization scheme is out of the scope of this work, we refer the interested reader to reference [24] for more information.

2.6 Resonators

A resonator, often also called cavity, is an arrangement of two or more mirrors between which light is reflected multiple times with minimal losses. It can be seen as a counterpart to an electrical resonating circuit in that it stores optical energy at frequencies which are determined by the specific configuration used. Possible configurations include two plane or spherical mirrors facing each other and more exotic configurations like ring or rectangular cavities. In this work we will only discuss the two mirror configuration, which is commonly used for stabilization purposes.

In this section we will first develop some insight into the topic by discussing the plane-mirror resonator before discussing the spherical configuration, which is usually used in practice. We will present some of the physics involved in these systems as well as some technical considerations one has to be aware of when actually working with one of these devices. For more information we suggest references [24] and [18].

2.6.1 The plane-mirror resonator

Figure 2.8 shows a two plane-mirror cavity, also called Fabry-Perot interferometer or etalon. Light inside the cavity will get reflected multiple times at the mirrors and the components from each round-trip will interfere with each other. After reaching a steady state (the reaching of the steady state and the response of the cavity to a change in the incident light field are out of the scope of this work and can for example be treated by using the Quantum Langevin formalism) only certain frequency components will have

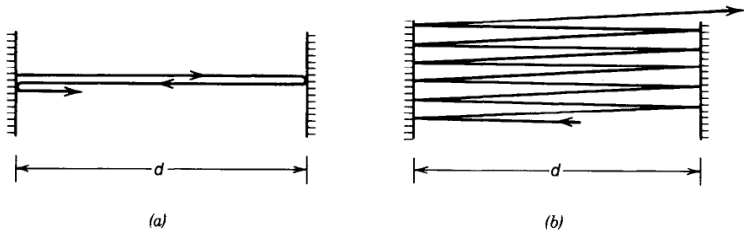

Figure 2.8: (a): Light is getting reflected multiple times in a plane-mirror resonator. The different components from different roundtrips interfere with each other, leading to a wavelength requirement for constructive interference. (b): A plane-mirror resonator is only stable for light perpendicular to the mirrors' surfaces and perfectly parallel mirrors. Figure taken from [18].

interfered constructively, while all others have been averaged to zero through the interference.

A standard way to mathematically tackle this situation is to solve the Helmholtz equation $\Delta U(\mathbf{r}) + k^2 U(\mathbf{r})$ for the complex amplitude $U(\mathbf{r})$ of the electric field under appropriate boundary conditions and the wavenumber k. For example, in the case of the lossless plane mirror the transversal component of the field has to vanish at the mirrors. For the sake of a simpler mathematical treatment, we will present a less rigorous and physically motivated approach of deriving the needed results.

The condition for constructive interference is that the lightwave has to repeat itself after a single round-trip in the resonator. This means that the accumulated phase-shift from a round-trip in the resonator has to be a multiple of 2π. The phase of a lightwave varies as kx, where $k = 2\pi n/\lambda$ is the wavenumber, n is the index of refraction, λ is the wavelength in vacuum and x is the distance travelled by the light, measured from the first mirror. This equation for the phase leads to the condition

$$k2d = q2\pi, \tag{2.16}$$

where q is an integer and d is the distance between the mirrors. The refractive index of the material inside the cavity influences this condition through the speed of light c.

Substituting the definition of the wavenumber and using $\nu = c/\lambda = c_0/(n\lambda)$, where c is the speed of light in the medium with refractive index n and c_0 is the speed of light in vacuum, we arrive at the condition

$$\nu_q = q\frac{c}{2d} \tag{2.17}$$

for the frequencies, that interfere constructively inside the cavity.

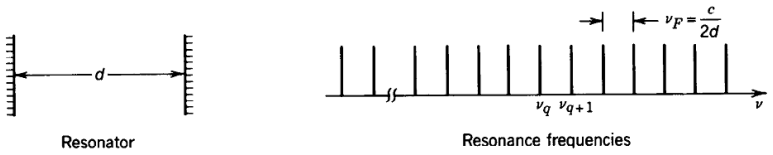

Figure 2.9: A plane-mirror resonator with a distance d between the mirrors will only resonate with light of certain resonance frequencies in its steady state while all other frequency components are averaged to zero by the interference. The resonance frequencies are multiples of the free spectral range $\nu_F = c/2d$, where c is the speed of light in the material feeling the space between the mirrors and d is the distance between the mirrors. Figure taken from [18].

This means that only light of certain resonance frequencies will survive in the steady state, while all other components are averaged to zero. The resonance frequencies are spaced by the so called free spectral range $\nu_F = c/2d$, which is determined by the index of refraction (through c) and the distance between the mirrors. A shorter cavity will have its resonance frequencies separated farther than a long cavity. The free spectral range is important to consider in practice when building a cavity, as it is oftentimes necessary to vary the frequency of the laser used over at least one spectral range. When using the PDH-technique it is important to choose a lower phase modulation frequency than the free spectral range of the cavity, as this would otherwise mean that there are additional resonances in the vicinity of the PDH error signal, making it unusable (see also sections 2.5 and 3.5.3).

When including possible losses at the mirrors, the condition 2.17 for lightwave-frequencies allowed inside the resonator is getting less stringent. This situation is depicted in figure 2.10, showing that a lossless resonator allows for a very good storage of light of frequencies satisfying Eqn. 2.17. A resonator with losses does sustain lightwaves of these resonance frequencies very well, but also allows for waves with frequencies near to those points to some lesser extent.

The form of the transmission peaks is given by Airy functions, which have the form

$$I(\nu) = \frac{I_{max}}{(1 + F/\pi)^2 (\sin \pi\nu/\nu_F)^2}, \tag{2.18}$$

the derivation of which is carried out in detail in reference [18]. Here ν_F once again depicts the free spectral range and ν the frequency. The finesse F and maximum intensity I_{max} will be discussed in the following paragraphs.

The maximum intensity is only reached at the frequencies ν_q of the lossless resonator and is given by

$$I_{max} = \frac{I_0}{(1 - |r|)^2}, \tag{2.19}$$

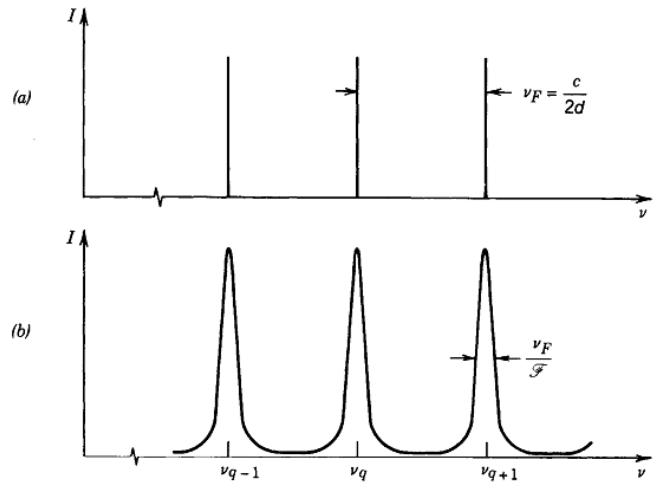

Figure 2.10: Top: A lossless resonator allows only light of certain frequencies ν_q (see Eqn. 2.17) to exist, light of all other frequencies interferes destructively. Bottom: A resonator with losses sustains the same frequencies very well, but also supports light of close-by frequencies to a lesser extent. The width of the peaks is determined by the free spectral range ν_F and the finesse of the resonator. Figure taken from [18].

where I_0 is the incoming intensity of the light and r is the reflectivity of the mirrors, assumed to be equal here. Thus the maximum intensity gives the height of the transmission peaks.

The quantity F in Eqn. 2.18 is called the **finesse** and is one of the most important quantities connected to a resonator. It is defined as

$$F = \frac{\pi\sqrt{|r|}}{1-|r|} \tag{2.20}$$

and is thus solely determined by the reflectivity r of the mirrors (assumed to be equal here). A higher reflectivity (less losses) consequently leads to a higher finesse of the cavity. As can be seen from analyzing the denominator of Eqn. 2.18 the finesse determines the width of the transmission peaks – the higher the finesse, the higher the reflectivity of the mirrors, the closer the resonator is to being perfectly lossless, the narrower the peaks.

This relation leads to another definition of the finesse through

$$F = \frac{\nu_{\text{fsr}}}{\Delta\nu}, \tag{2.21}$$

where ν_{fsr} is the free spectral range of the resonator and $\Delta\nu$ is the full-width-at-half-maximum width of the resonators transmission peaks.

Because the absolute width of the transmission peaks is posing a fundamental limit to stabilization schemes when the transmission peaks are used as a frequency reference (see for example Eqn. 2.15 for the PDH-scheme), it is of utmost importance to choose the relevant quantities in an appropriate way to fit the application. As the absolute width of the peaks is determined by the ratio ν_F/F of the free spectral range to the finesse, one should calculate the required values to achieve the desired frequency limit.

Example: For the first stabilization step, we want to achieve around 10 kHz linewidth by stabilizing the laser on a transmission line of a cavity. The cavity has a physical length of $d = 15\,\text{cm}$ and thus a free spectral range of $\nu_F = c/2d \approx 1\,\text{GHz}$. Assuming active stabilization manages to stabilize the frequency to a percent of the peaks width[7], we need an absolute peak-width of around at least 1 MHz, requiring a finesse of at least 1000. As we want to allow for some technical imperfections, we decided to raise the finesse of the kHz-cavity (for more details, see Sec 3.5) to 3000.

2.6.2 Measuring the finesse

Because the finesse is such an important property, this section discusses two ways of measuring it experimentally.

One way to characterize the finesse of a resonator is to scan the laser's frequency over a transmission peak (see Fig. 2.4) and to measure the transmitted light through the cavity (or the light reflected from the cavity). If the laser's linewidth and the free spectral range of the cavity is known, the finesse can be determined from the width of the transmission peak. The difficulty with this approach is the mathematical treatment as well as knowing the laser's linewidth accurately enough.

The laser's linewidth can often be modelled by a Voigt-function, due to the interplay of the Lorentzian-contribution arising from the natural linewidth of the involved laser transition and the Gaussian-contribution from different random effects which broaden this Lorentzian linewidth. The function which describes the transmission peaks of a cavity are Airy-functions (see Eqn. 2.18 and Fig. 2.10).

The influence of the laser's linewidth on the width of the measured transmission peak can be easily understood by looking at two extreme cases. In the case of a infinitely broad laser linewidth there will always be light transmitted through the cavity, giving a measured transmission peak of infinite width. In case of a infinitely narrow laser linewidth the measured transmission will be exactly the transmission function of the cavity. These extreme cases demonstrate that the laser can have significant effect on the measured

[7] The active stabilization keeps the frequency of the laser at a specific setpoint of the transmission peak. Usually active stabilization can keep the frequency stable to a percent or less of the functions width, depending on the functions form, the stabilization used and technical details.

transmission through the cavity.

Mathematically the resulting transmission $T(\nu)$ through the cavity is given by the convolution of the transmission function of the cavity (Airy-function) and the laser's linewidth function (typically Voigt-function). As the transmission $T(\nu)$ is the measured quantity and the linewidth function is assumed to be known, one has to determine the Airy-function by de-convolution. Often it is useful as an approximation to replace the Voigt-function and the Airy-function through Gauss-functions, as those are relatively similar and simplify the involved mathematics considerably.

Specifically the convolution of two Gaussian functions with standard deviations σ_1 and σ_2 gives, again, a Gaussian function with standard deviation

$$\sigma_3 = \sqrt{\sigma_1^2 + \sigma_2^2}. \tag{2.22}$$

The standard deviation of a Gaussian function is related to its full width at half maximum (FWHM) through

$$\mathrm{FWHM} = 2\sqrt{2\log 2}\sigma. \tag{2.23}$$

This procedure allows for a quick but rough approximation of the linewidth.

Another way of measuring the finesse is by a ring-down measurement. This technique relies on the fact that a high-finesse resonator on resonance will store the light for a long time even if the laser source is turned off. By measuring the transmission decay and by using the Fourier relation between the time- and frequency-domain, one can determine the linewidth of the resonator. In this technique the laser's linewidth does not play a role, because the characteristic time for which light is stored by the cavity is solely determine by the resonator.

It turns out (see for example section 10 in Ref. [18]), that the light transmitted through the cavity will decay as

$$T(t) = \exp\frac{-t}{\tau}, \tag{2.24}$$

where t is time and τ is the characteristic decay timescale of the resonator. By using the Fourier relation 2.3 this corresponds to a linewidth function of

$$T(\nu) = \frac{1}{1 + i4\pi\nu}, \tag{2.25}$$

which has a full-width-half-maximum of $\Delta\nu = 1/2\pi\tau$.

The finesse can then be found through the relation

$$F = \frac{\nu_{\mathrm{fsr}}}{\Delta\nu}, \tag{2.26}$$

where ν_{fsr} is the free spectral range.

2.6.3 The spherical-mirror resonator

As the plane-mirror configuration, discussed in the preceding section, is highly prone to misalignment (see for example figure 2.8), oftentimes spherical mirrors are used. A spherical mirror resonator consists of two mirrors with radii of curvatures R_1 and R_2, facing each other at a distance d. A concave mirror has a negative radius of curvature while a convex mirror has a positive radius of curvature. The plane-mirror resonator is a special case where the radii of curvature tend to infinity.

The spherical mirror resonator can, for example, be analyzed through the use of ray matrix methods. As the exact treatment of this problem is out of the scope of this work, we will resort to presenting some of the most important results and discuss them in the context of this project.

Stability of the spherical-mirror resonator

Compared to the plane-mirror resonator, which needs perfectly parallel mirrors to create a stable configuration, there is more room for error in case of the spherical-mirror resonators. But while the spherical mirror resonator is more stable against mirror misalignement, there are some additional restrictions concerning the distance of the mirrors.

This can be understood in the following way: To create a stable resonator configuration, light rays have to traverse the same path over and over again, either after one or another fixed number of round-trips. This allows for a steady state and constructive interference for light of certain frequencies and position/inclination – just as in case of the plane-mirror resonator.

As the laws of ray optics teach us that a spherical mirror has a focal point at a distance of half the radius of curvature from the apex and that parallel ray gets converted to a focal ray, it is clear that two spherical mirrors of radii of curvature R at a distance $-R$ are a stable configuration (remember that convex mirrors have a negative radius of curvature). The focal point is positioned at the midway between them and every parallel ray is reflected through this focal point of both mirrors to give another parallel ray after reflection at the other mirror, repeating its way after four reflections. This special configuration is called **symmetric confocal** and has some very special properties, which we will come back to in the appropriate sections.

Clearly, changing the distance of the mirrors very slightly compared to the confocal configuration will still give a stable configuration, while putting the mirrors at a huge distance, much bigger than the radii of curvature, from each other will clearly create an unstable configuration as a light ray reflected at one mirror will never even hit the other one.

If analyzed thoroughly one can find a stability condition of the form

$$0 \leq \left(1 + \frac{d}{R_1}\right)\left(1 + \frac{d}{R_2}\right) \leq 1, \tag{2.27}$$

which is often expressed in terms of the g-parameters $g_i = (1 + d/R_i)$ as

$$0 \leq g_1 g_2 \leq 1. \tag{2.28}$$

For stabilization purposes one usually uses a configuration close to the confocal configuration. Why the confocal configuration itself is not useable for this type of application is discussed in the next Sec 2.6.4 about modes. While one may think that any configuration near the confocal configuration is stable this is **only true for symmetrical configurations**. The reason for this will become clear in the next section, but we want to emphasize here, that a configuration with **two different mirrors will have an unstable configuration near the confocal configuration**. This fact means that a cavity consisting of mirrors with radii of curvature $R_1 = 15\,\mathrm{cm}$, $R_2 = 20\,\mathrm{cm}$ and a distance of $d = 15\,\mathrm{cm}$ will be unstable, which may not be obvious at first glance (it definitely was not to us).

2.6.4 The modes of the spherical mirror resonator

A resonator mode is a lightfield, which can exist inside the resonator when the stable state of the resonator has been reached. For this to happen, the light field has to have a special geometry as well as frequency, because different round-trips of the lightfield between the mirrors of the resonator have to interfere constructively. This criterion means that the lightfield has to retrace its path inside the resonator after a fixed amount of round-trips inside the resonator and its phase has to be a multiple of 2π at the same time. Light that does not satisfy both conditions will interfere destructively over the many round-trips inside the resonator and thus not exist inside the resonator. This section will discuss the modes of the spherical mirror resonator and the modes' resonance frequencies.

In case of the spherical mirror resonator one of the simplest cases is a light wave, whose wavefronts' curvature does match the curvature of the mirrors at the position of the mirrors. In this case the wavefront retraces its path, satisfying the first condition for a resonator mode. Incidentally a Gaussian beam or a Hermitian beam, which are also used in modelling laser beams, have spherical wavefronts at distances larger than one Rayleigh range from the laser's focus point[8]. This fact means that Gaussian- or Hermitian modes are oftentimes modes of the spherical resonator, provided there is a focus position and a waist size for the mode so that the resulting curvature of the wavefront matches the mirrors' curvatures at their respective positions.

Provided a focal position and waist has been found so that the wavefronts' curvatures match the mirrors's curvatures at the position of the mirrors (see figure 2.15), the lightfield will retrace its path, satisfying the first condition for the existence of a mode. To satisfy the second condition, the lightwave

[8] See for example chapter 3 in [18].

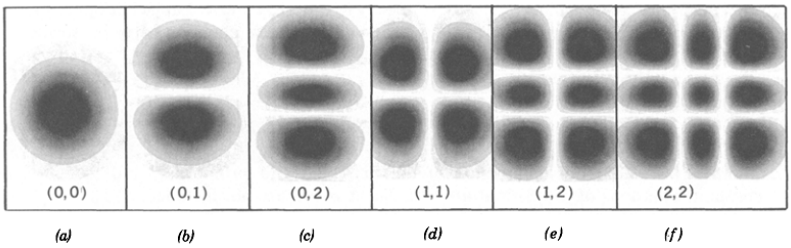

Figure 2.11: Intensity distribution in the (x,y)-plane of some low order Hermitian-Gaussian beams, when z is the propagation direction. The order (l,m) is given beneath each distribution. Figure taken from [18].

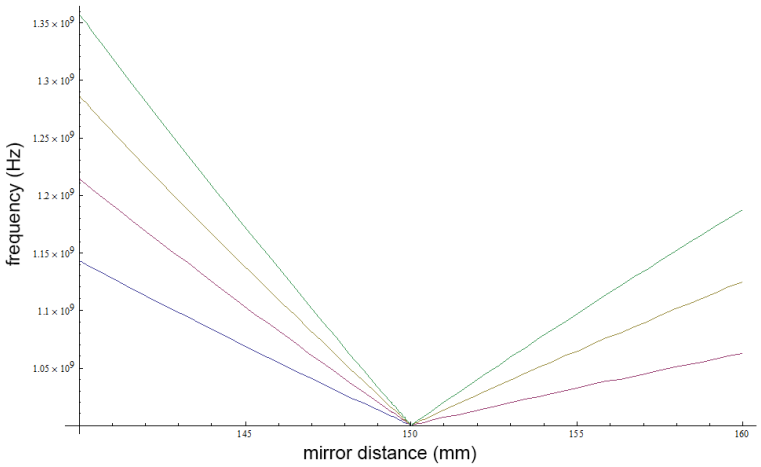

Figure 2.12: Resonance frequencies of Hermitian-Gaussian modes with different (l, m), when both mirrors have a radius of curvature of 150 mm. At the confocal configuration, where the distance of the mirrors is equal to the radius of curvature, all modes of different (l, m) have the same resonance frequency.

needs to pick up a phaseshift of $n2\pi$, where n is an integer, in one round-trip. Only light of special resonance frequencies will satisfy this condition and thus be modes of the spherical resonator. Hermitian-Gaussian beams of different frequencies will pick up phaseshifts different from $n2\pi$ in one round-trip and thus interfere destructively over many round-trips.

While the wavefront form is the same for every Gaussian- or Hermitian beam of order (l, m) their phase behaviour is different in the way that they have a different Gouy phase shift, depending on l and m. This fact means that different orders (l, m) of Hermitian-Gaussian-modes will in general have different resonance frequencies.

The phase of a Hermitian-Gaussian beam of order (l, m) on the beam axis is

$$\phi(0,z) = kz - (l+m+1)\zeta(z), \tag{2.29}$$

where z is the distance from the focus in propagation directions, $k = 2\pi/\lambda$ is the wavenumber, λ is the wavelength, $\zeta(z) = \tan z/{z_0}^{-1}$ and $z_0 = \pi W_0^2/\lambda$ [18].

After the single round-trip the phase must be an integer multiple of 2π:

$$2kd - 2(l+m+1)\Delta\zeta = 2\pi n, \tag{2.30}$$

where n is an integer, $\Delta\zeta = \zeta(z_2) - \zeta(z_1)$ with z_1, z_2 the position of the mirrors and d is the distance of the mirrors.

When rewriting the wavenumber $k = 2\pi\nu/c$ in terms of the frequency ν and the speed of light c and introducing the free spectral range $\nu_f = c/2d$, we find the resonance frequencies $\nu_{l,m,n}$ as

$$\nu_{l,m,n} = n\nu_f + (l+m+1)\frac{\Delta\zeta}{\pi}\nu_f. \tag{2.31}$$

Modes of same (l, m) but different n are called **longitudinal modes** and are spaced by the free spectral range $\nu_f = c/2d$. They have the same spatial distribution in the (x,y)-direction. Modes of different (l, m) but same n are called **transverse modes** and have different intensity distributions in the (x,y)-direction (see Fig. 2.11 and Fig. 3.11).

In the special case of the confocal configuration all modes of same n have the same resonance frequency, making this configuration unsuitable for laser stabilization purposes, where one wants to lock to one and only one mode of the cavity as a frequency reference. Figure 2.12 shows the mode spacing as a function of the mirror distance for a cavity made up from mirrors with radii of curvature $R_1 = R_2 = 150\,\mathrm{mm}$.

The parallel between the modelling of a laser beam as Gaussian- or Hermitian-beam and the fact that those are modes of the spherical mirror resonator means that there exists an easy way to optimize the laser's coupling to a specific mode. This procedure is called **mode-matching** and relies on the idea of making the laser beam's properties as similar as possible to the properties of the mode one wants to match to. In the case of the Hermitian-Gaussian modes this means optimizing the laser's focus, waist and Rayleigh length to match the mode's properties as closely as possible. This procedure will lead to the laser coupling to a certain mode in a dominant way, while other modes are suppressed.

2.6.5 The instability of asymmetric mirror resonators near the confocal configuration

As discussed in the previous sections a confocal mirror configuration is not the optimum configuration for stabilization purposes as all the spatial

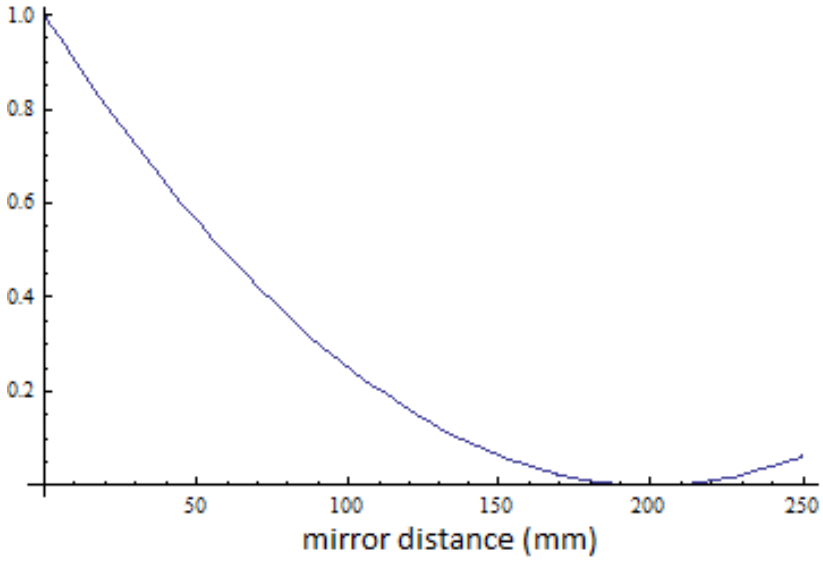

Figure 2.13: The stability condition (Eqn. 2.28) for mirrors with radii of curvature of $R_1 = 20\,\text{cm}$, $R_2 = 20\,\text{cm}$ as a function of mirror distance. There is no unstable configuration until very large distances.

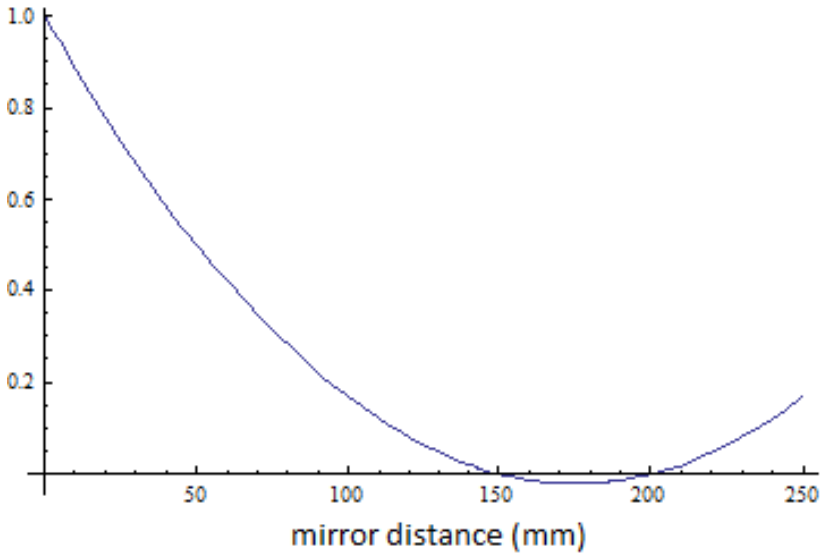

Figure 2.14: The stability condition(Eqn. 2.28) for mirrors with radii of curvature of $R_1 = 20\,\text{cm}$, $R_2 = 15\,\text{cm}$ as a function of mirror distance. Configurations for $15\,\text{cm} \leq d \leq 20\,\text{cm}$ are unstable.)

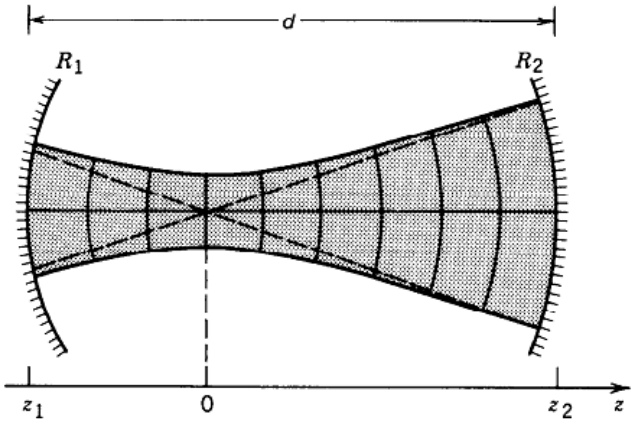

Figure 2.15: Sketch of the laser beam, modelled by a Gaussian beam, inside the cavity. If the wavefront of the light matches the curvature of the mirror at the position of the mirror, the light will retrace its path and create a stable mode. If no focus can be found so that the wavefronts match the curvature of the mirrors at both mirrors, the resonator is unstable. Figure taken from [18].

Hermitian-Gaussian modes exist at the same resonance frequency, which creates problems like cross-talk between modes and shifting intensity patters, among many others. To create an appropriate mode spacing one usually slightly deviates from the confocal configuration, for example through moving the mirrors or slightly changing the radii of curvature. Interestingly a symmetric resonator has no unstable configuration in the vicinity of the confocal configuration while a asymmetric resonator has an unstable area, making the cavity unusable for stabilization purposes!

In similar projects in the last years we used two mirrors with $R = 15\,\mathrm{cm}$ on a 10 cm spacer for our stabilization cavities. For this project and the involved two-stage stabilization, we planned to change the distance between the mirrors to 15 cm to decrease the free spectral range to half the initial value. This was deemed easier to work with, because this cavity had to be scannable over at least a free spectral range (see Sec 3.5 for more details).

The new spacer would give a confocal configuration when the old mirrors were used, so we changed a mirror to 200 mm to deviate slightly from the confocal configuration and reach a suitable mode spacing. As it turns out, this creates an unstable configuration, totally unusable for our application. In the end we had to redo the cavity using mirrors with $R = 20\,\mathrm{cm}$ and the same spacer of 15 cm.

The stability condition for the two situations are shown in figures 2.13 and 2.14. Clearly the asymmetric configuration is unstable at distances between 15 cm and 20 cm. This is because of the following reason: In a stable

configuration the lightfront of a certain mode has to retrace its steps after a fixed amount of round-trips. The simplest way this can happen is if the curvature of the light-mode is the same as the radius of curvature at the position of the mirror. Then the wavefront reaches the mirror surface at the same time and is reflected in the same way, retracing its way backwards.

For a symmetric configuration this is very easily accomplished because the laser beam behaves like a Gaussian beam, meaning it is symmetric around its focal point. This fact means that the focal point has to lie in the middle between the two mirrors for symmetry reasons in the case of a symmetric resonator configuration.

However, for asymmetric configurations it can happen that there is no position for the focal point so the curvature of the light's wavefronts is the same as the radius of curvature at **both** mirrors. In this case one can find, for a laser beam of certain waist and Rayleigh-length, a focal position so that the wavefront's curvature matches the mirror's curvature at one and only one of the mirrors. This is what causes the instability shown in figure 2.14.

Chapter 3

Experimental setup and results

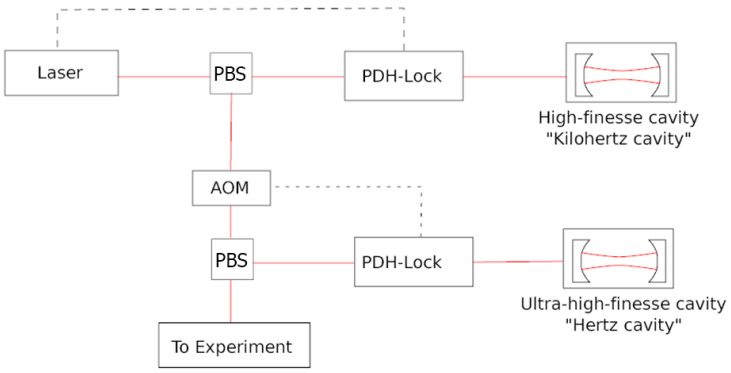

Figure 3.1: Sketch of our two-stage stabilization setup. The laser is first pre-stabilized onto the kHz-cavity, using a PDH-lock with laser current as actuator. A part of the light is split off through a polarizing beam splitter (pbs) and sent to the experiment and to the Hz-stabilization stage. The Hz-lock uses a separate PDH-lock with an acousto-optic modulator (AOM) as actuator.

3.1 Two-stage stabilization setup

As described in the theory section (2.5) the Pound-Drever-Hall(PDH) locking-scheme to a cavity is a common way to decrease the linewidth of a laser by active stabilization. While achieving a linewidth of 10 kHz can be achieved with moderate effort, it has proven more challenging to reduce the linewidth even further. The reason for this is that sufficiently stable references, like cavities, were extremely difficult and expensive to build. Only very few laboratories around the world had the knowledge and resources to realize such systems (see also chapter 1).

In recent years, technological improvements and research advancements [1?] have led to highly stable reference cavities at more affordable prices, allowing more laboratories access to ultrastable lasers with linewidths in the Hertz regime. Today there are even commercial vendors, like stable laser systems, offering these high performance reference cavities to any laboratory interested. The ultrahigh-finesse cavity in this work was purchased from stable laser systems.

While it is possible to use the PDH scheme to directly lock to such a cavity, we have decided to instead use a two-stage stabilization setup. As shown schematically in figure 3.1, we are using a cavity with a finesse of around 3000 (which will be referred to as kHz-cavity from now on) to prestabilize the laser linewidth to around 10 kHz. Then the laser is locked to a ultrahigh-finesse cavity with a finesse of $\approx$ 200000 (from now on referred

to as Hz-cavity) using a separate PDH lock, decreasing the linewidth to the 10 Hz level.

While the final performance in terms of linewidth is dominantly determined by the finesse and stability of the Hz-cavity and should therefore be comparable in both, the single- and two-stage stabilization-scheme, we expect the overall system to be much more stable and easier to optimize in the two-stage setup. Because the kHz-locking stage is counteracting the noise above $\approx 10\,\mathrm{kHz}$[1], the Hz-locking stage has only to worry about noise components in the range up to this frequency. This fact means that the requirements for the servo-system of the Hz-stage are less demanding (as signal delay limits the servo systems bandwidth) and separates the frequency ranges for the two stages, allowing separate optimization of parameters.

As the kHz-cavity needs to counteract noise of very high frequency in the MHz-range and above, we use the current of the laser diode as actuator, as well as the internal grating for lower frequencies. The current driver itself allows for modulation up to tens of Megahertz (see [28]), which means that the actually achievable bandwidth is usually limited by the diode itself and is supposed to be around $1 - 5\,\mathrm{MHz}$ in our case [28].

The Hz-lock needs a separate actuator, which is independent from the kHz-lock. We are using an 110 MHz acousto-optic modulator (AOM) – even though this device is usually used to shift the lasers frequency by a fixed amount, it can also be used to modulate the light's frequency, thereby acting as actuator (see also Sec 2.3 for an explanation why a time-varying shift of the frequency can change the linewidth.).

The bandwidth of an AOM, given by

$$B = \frac{1}{T} \text{ with } T = \frac{D}{v_s}, \tag{3.1}$$

is limited by the time T the soundwave of velocity v_s in the crystal needs to pass the distance D between the piezo-crystal and the end of the laser beam [18] (so the soundwave has to traverse the distance to the laser beam and the full diameter of the laser beam itself).

In-loop behaviour is modified by the time the signal needs to go around the loop to reach the AOM again. If one would lock directly to the Hz-cavity, using the AOM as an actuator, the bandwidth might pose a problem, but as we are dealing with a linewidth of 10 kHz after the first lock, we at most need a bandwidth of several tens of kiloHertz, which is easily achieved.

Example: A beam diameter of 0.3 mm and a distance from the piezo gives $D = 0.5\,\mathrm{mm}$. Together with the the velocity of sound of fused quartz $6\,\mathrm{km/s}$ this results in a bandwidth of $\approx 12\,\mathrm{MHz}$. Three metres of cable for the loop limit have a round-trip time of 30 ns, assuming the signal travels at 2/3 of the speed of light[2],

[1] Remember that the bandwidth of the PDH locking scheme is not determined by the cavities bandwidth – otherwise this would be impossible (see also).

[2] See for example http://www.epanorama.net/documents/wiring/coaxcable.html.

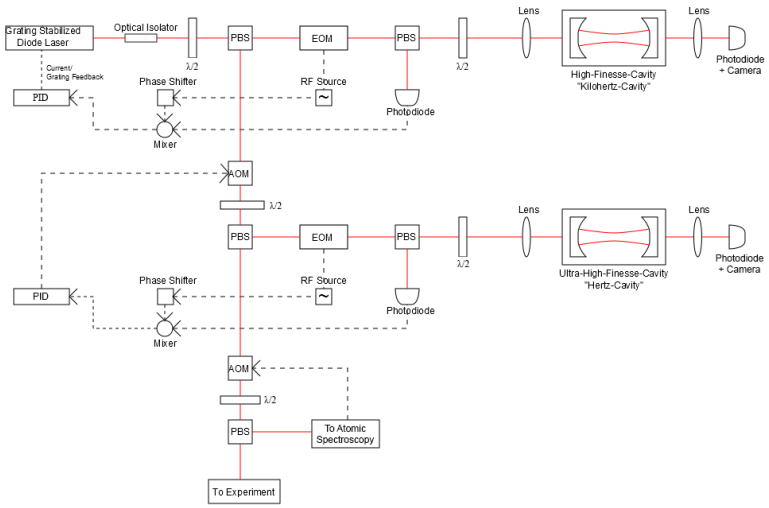

Figure 3.2: Sketch of the key parts of our setup.

limiting the bandwidth to $\approx 66\,\mathrm{MHz}$.

Another advantage of the two-stage stabilization-scheme is that it allows for different modulation frequencies in the two stages. This is can be advantageous because sometimes the modulation frequency in the PDH-scheme can not be made arbitrarily high, in case there are other modes near the mode one tries to lock to (see also chapter 3.5). As the modulation frequency determines the capture range of the PDH-locking scheme, this can lead to an increased capture range of the total lock compared to the single-stage setup. For example, this is the case when the modulation frequency of the kHz-stage can be made higher than the one of the single-stage (in the two-stage setup, usually the kHz-lock determines the capture range).

The downside of the two-stage setup are obviously the increased costs, the need for more infrastructure (amplifiers, rf-generators etc.) and the additional time for setup. The space requirements approximately double to about two $60x60\,\mathrm{cm}^2$ breadboards plus external components.

3.2 Overview over the setup

This section will give a short overview over each part of the setup and its interplay with the other parts, while the details about each subpart will be presented in the respective sections. Figure 3.2 shows a sketch of the most important parts of the setup.

The laser is a Toptica DL 100 pro diode laser, which emits light of 698 nm

wavelength with a linewidth less than 1 MHz [28]. The frequency can be controlled through current modulation and through controlling the piezo inside the laser (see Sec 3.3 for more details).

The light then passes a 60 dB optical modulator by Qioptiqs to stop back-reflection of any kind to reach the laser. Back-reflections would create an additional feedback to the system and disturb the stabilization process in an unpredictable way.

The light is then split up into different branches by using $\frac{\lambda}{2}$-waveplates, followed by polarizing beam splitter cubes and $\frac{\lambda}{2}$-waveplates before fibre couplers. Polarization maintaining, single mode fibres take the light to the different parts of the setup and clean the mode to a Gaussian beam profile.

One part of the light is used to stabilize the laser to the kHz-cavity via a standard Pound-Drever-Hall lock (see Sec 2.5 and [27]). The light passes a home-made electro-optic modulator, running at a frequency of 34.1 MHz. The signal is created by a home-made direct-digital-synthesizer system (DDS) and a home-made rf-amplifier with a gain of 40 db at 10 MHz. This creates additional frequency components in multiples of the modulation frequency from the carrier, see also Sec 2.3 and figure 2.3. The modulation depth for this process is ≈ 1, which means that the first sidebands are dominant, with a power of around 40-50% of the carrier's.

The light is then sent onto the kHz-cavity, which has a finesse of around 3000. The reflected light is monitored by a 120 MHz home-made photodiode, creating the signal for the PDH-stabilization scheme. The transmitted light is monitored by a black and white camera for qualitative information, as well as a photodiode, which is used for optimizations and measurements.

The signal from the reflected light is then mixed with the local oscillator to give the PDH error signal. This signal is then low-pass filtered and fed into the FALC-controller, which is a special PID-controller by Toptica. The output signal of this controller is then fed back to the laser current and the grating's position, inside the laser, to complete the feedback loop and stabilize the laser.

The part of this stabilized light is split off for the PDH-lock onto the Hz-cavity, passing an 110 MHz acousto-optic modulator by Crystal Technologies. This AOM will be used as an actuator for the Hz-stage and is driven by a Rohde und Schwarz signal generator with external modulation input.

While the Hz-lock is set up mostly identically to the kHz-lock, there are the following differences. The electro-optic modulator is a PM-C-BB with sine amplifier by Qioptiqs, running at a frequency of 10 MHz. The signal for this is also created by the home-made DDS system and the same home-made rf-amplifier as in case of the kHz-setup. The PDH-signal is created in the same way and sent to a separate FALC-controller. The output signal is then fed into the external modulator input of the Rohde and Schwartz signal generator, driving the AOM, thus completing the feedback loop and

stabilizing the laser.

3.3 The Toptica DL 100 pro

For our experiment we use a Toptica DL 100 pro laser, which is a external cavity diode laser with a special Littrow-Hänsch-type grating stabilization. The laser is mounted onto the steel optical breadboard by using a suitable baseplate to achieve the desired beam height. The baseplate and the mounting screws are electrically isolated from the optical table to prevent ground loops.

According to Toptica the laser has a linewidth of less than 1 MHz and can be tuned over tens of nanometres without realignment. While none of those properties were measured directly, we did not find any indication to believe otherwise. The laser can be tuned continuously by directly changing the temperature and current on the laser control module, with only rare occasions of multi-mode behaviour. These can be resolved by finding another combination of temperature and current leading to the same wavelength but single-mode behaviour.

To protect the laser from reflections, which would lead to an additional feedback mechanism and thereby potentially degrading stability, we added a 60 dB optical isolator, produced by the company Qioptiqs, formerly Linos. The optical isolator is mounted inside the laser housing, directly after the output of the laserhead. The optical isolator needs to be optimized in orientation with respect to the laser's polarization. After the optical isolator the laser has a maximal output of around 15 mW.

The DL 100 pro offers two modulation inputs (AC- and DC-coupled), which can be configured to serve different purposes by setting internal jumpers. For our stabilization scheme we use the DC-coupled modulation input in standard configuration. This configuration allows for a modulation bandwidth of up to 50 MHz. In practice however, the available modulation bandwidth is determined by the diode used and is expected to be less than 10 MHz.

The laser can be scanned with the use of a scan module by Toptica, which controls the piezo's position, as well as the current and temperature. The scan module allows for easy tuning of the laser's wavelength through the offset knob and easy scanning at different frequencies and ranges. Scanning the laser will not only vary the frequency but also the power, because the output power of a laser diode depends on the current and temperature, which are quantities that are scanned. The scan needs comparable time to increase the frequency as it does to decrease it.

For more information see the technical manual for the DL 100 Pro series supplied by Toptica [28].

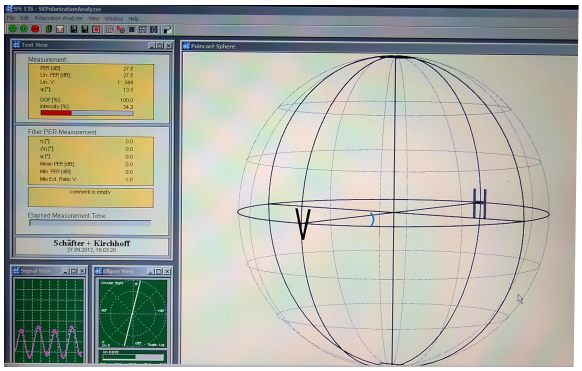

Figure 3.3: Photograph of the software for the polarimeter. The polarisation is represented by a Poincaré sphere, while the blue dots are the actual polarisation measurements, taken at certain time intervals.

3.4 Fiber coupling and beam shaping

We use single-mode, polarization maintaining fibers from Thorlabs and collimators from Schäfter + Kirchoff to transport the laser light to the different parts of the setup (kHz-lock, Hz-lock and a Fabry-Perot etalon for testing). This also ensures clean Gaussian beam profiles after the fibres.

At the output of the laser the beam profile is non-Gaussian, as is typical for diode lasers, due to the typical geometries for the diodes. The fact that the beam profile is not Gaussian degrades the coupling efficiency into the fibers, because the used polarization maintaining single mode fibers only conduct TEM00-modes (which have a Gaussian beam profile) with size appropriate for the respective type of fiber.

Without beam shaping we obtain fiber coupling efficiencies of 60%, 53% and 67% for the three fibers in our setup, where the fibers go to the Hz-stage, a Fabry-Perot etalon for testing and monitoring purposes and the kHz-stage. The respective changes in polarization, due to warming of and strain on the fiber are 1.5°, 1.7° and 0.8°.

3.4.1 Finding the right polarization angle for coupling

It is important that the light is entering the fibers with a longitudinal polarization in the direction of the fiber axis. Only then is the fiber polarization maintaining and will not change the polarization of the outgoing light due to strain or temperature variations somewhere along the fiber. As we use polarizing beam splitters after the fibers, these polarization changes would be translated into intensity changes into the different branches of the beam splitter.

One can find the right angle for the polarisation of the light to couple into the fiber through the following procedure: Assuming linearly polarized

light, we put a $\frac{\lambda}{2}$-waveplate in front of the fiber and a $\frac{\lambda}{2}$-waveplate and a polarizing beam splitter after the fiber. Both branches after the splitter are measured by a photodiode. The waveplate after the fiber is adjusted in a way that both beam splitter paths hold 50% of the light's intensity, which ensures maximum sensitivity to changes. Now, one warms a part of the fiber (for example, just holding them with your hands for some seconds) and monitors the change in intensities. If the angle at the first waveplate is wrong, the warming of the fiber will change the polarization of the outgoing light, thereby changing how much light goes into the separate branches of the beam splitter. One then changes the angle of the first waveplate to a new angle, readjusting the second waveplate to have 50% light in each branch and repeats the procedure. As soon as the intensity ratio at the beam splitter stays the same even when warming or twisting the fiber, the correct angle has been found.

Another way is to use a polarimeter, as can be seen in figure 3.3. This basically saves the setup after the fiber, one plugs in the fiber, adjusts the waveplate in front of the fiber and observe the change in polarization when warming or applying strain to it. Usually one can minimize the change in polarization to less than 2°. If this is not possible one should check that the fiber coupling efficiency is reasonable and the fiber as well as the collimator are clean.

3.4.2 Beam shaping

As the beam-profile after the fiber will always be determined by the geometry of the fiber, beam shaping before the fiber is only a question of fiber coupling efficiency. We have considered two ways of beam shaping the laser to a a more Gaussian beam profile but have found that, due to intrinsic losses in the methods, this does not give significant improvement in overall available light[3].

We have tried using a anamorphic prism pair to improve the beam profile. The working principle of the prisms is illustrated in figure 3.4. The problem of this setup is that light gets lost at each surface, thereby reducing the amount of useable light. We measured a power after the prisms of 15 mW with an input power of 18 mW, corresponding to a loss of 17%. While the coupling efficiency increases around 10%-15%, this still gives less useable light than directly coupling the laser into the fibers.

The second way of beam shaping we considered was the use of cylindrical lenses. As the width of the laser in the horizontal axis is about 3 times the vertical width, the idea is to build a telescope from cylindrical lenses, that changes one of those axis appropriately. The problem with this setup is that there are possible backreflections from the cylindrical lenses into the

[3] The fiber coupling efficiency itself obviously increases but as there is less light arriving at the fiber, this does not give any increase in useable light.

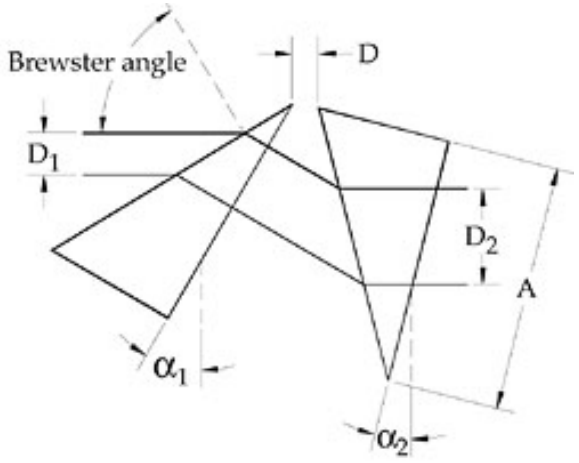

Figure 3.4: Sketch of the working principle of the anamorphic prism pair. One dimension of the beam gets changed while the other one is left undisturbed. This can be used to transform an elliptical beam into a circular one. Figure was taken from [29].

laser, which creates additional noise and instability – something which is detrimental to the purpose of this setup. As the amount of back reflection and the induced problems are only very hard to quantify, we only spent about three hours setting up the telescope and finding an overall increase of less than 1 mW in useable power. As this application's goal is about stability and not so much about maximizing laser output, we decided that the risk was not worth taking.

3.5 kHz-cavity

In this section we will describe the setup for the first stabilization stage, whose purpose is to reduce the linewidth to around 10 kHz. The design for this cavity and the surrounding chamber is based on a similiar project [30] in our group, most notably work from Bo Huang, Meng Khoon Tey, Simon Stellmer and Florian Schreck.

3.5.1 Experimental details of the kHz-cavity

The cavity itself consists of a $L = 15\,\mathrm{cm}$ Zerodur spacer, which is a material with an extremely low temperature expansion coefficient of the order of $10^{-8}\,\mathrm{K}^{-1}$. As shown in figure 3.5 this spacer features an axial drill, determining the optical axis of the cavity, and an additional drill to allow the air inside the spacer to escape when pumping down to vacuum.

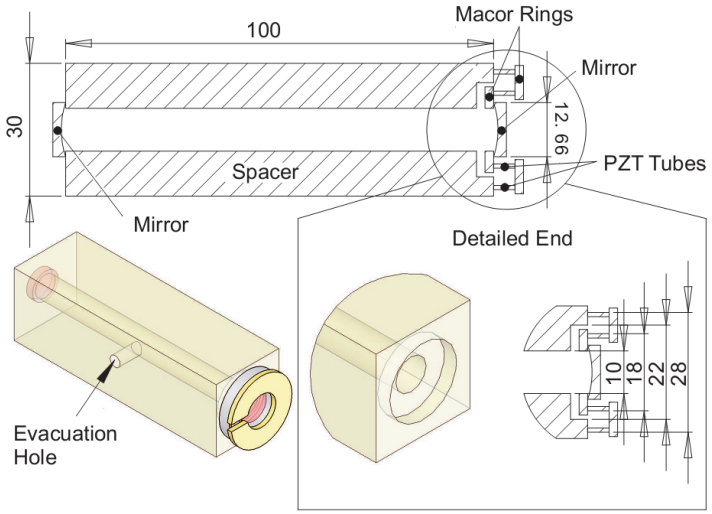

Figure 3.5: Sketch of the kHz-cavity with units in millimetres. Lower right: special construction to compensate for the relatively high temperature expansion coefficients of the piezo and Macor materials. Figure taken from [30].

Two identical mirrors[4] with a reflection coefficient of 0.999 and radius

[4] Produced by the company LayerTec.

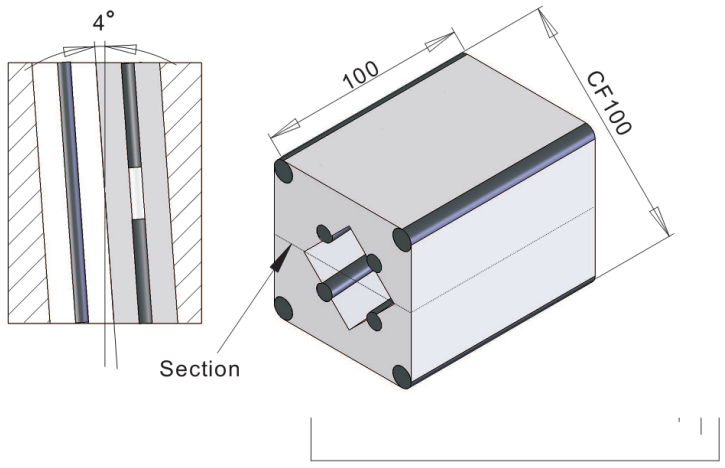

Figure 3.6: Schematic drawing of the stainless steelblock. In the current version, the inclination angle is reduced to 2° and we are using smaller parts of vitons rods to decrease strain and outgassing. Figure taken from [30].

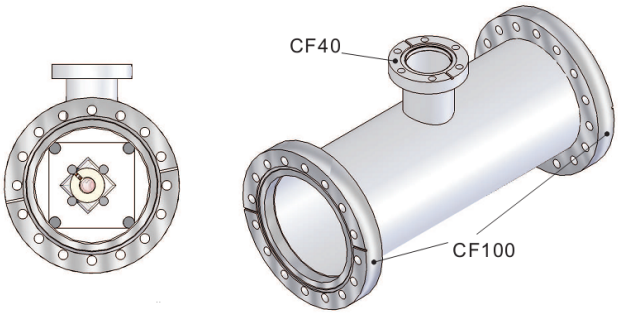

Figure 3.7: The vacuum chamber is made from a CF100 tube with two CF100 flanges at each end for the optical windows. The current version is custom-made and has two additional CF40 flanges and a CF60 flange on top of the chamber. These are used for mounting the electrical feedthrough, the ion pump and the valve for pumping down the chamber. Figure taken from [30].

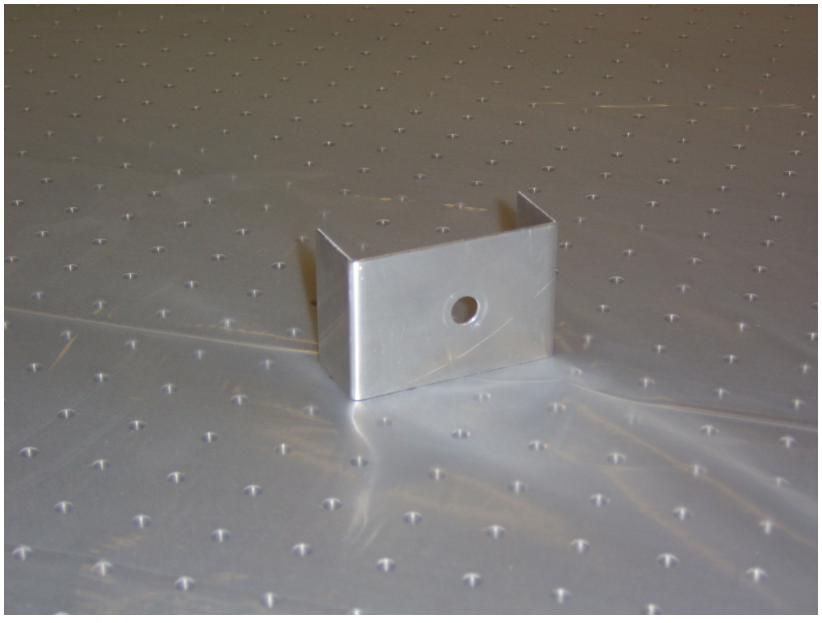

Figure 3.8: Photograph of one of the blackbody radiation shields. It consists of aluminum, bent into an U-shape, and is clamped at four points to the steelblock.

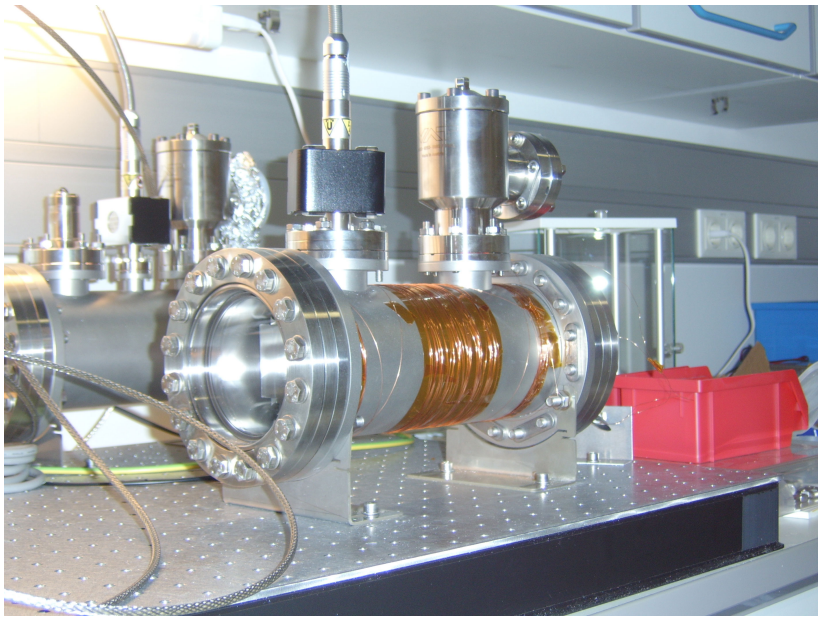

Figure 3.9: Photograph of the two vacuum chambers (without insulation) with cavities inside and valve and ion pump on top. The right one contains a cavity without piezo and shows the additional heating wires, usable for temperature stabilization. The left one contains a cavity with piezo, recognizable by the electrical feed-through on top. In our experiment we are currently using the cavity with the piezo, because it gives additional tunability.

of curvature of 20 cm are making up the cavity, letting us expect a finesse of around 3000 from Eqn. 2.21. With Eqn. 2.21 and a free spectral range of $c/2L = 1\,\mathrm{GHz}$, this gives an estimated width of 300 kHz for the transmission peaks of the modes (see Sec 3.5.3 for experimental measurements). The mirrors are directly glued to the spacer, using the special, heat curing, vacuum epoxy ND353 by Epotek, which has a sufficiently low outgassing rate to achieve a vacuum better than 10^{-7} mbar.

The disadvantage of this setup is that the length of the cavity cannot be controlled, which means that the absolute position of the transmission peaks can not easily be changed. While the position can still be tuned somewhat by controlling the temperature of the surrounding vacuum chamber, the low temperature expansion coefficient (from now on referred to as CTE) of the Zerodur[5] makes it challenging to move the position of the transmission peak over a significant part of the free spectral range. This inability to tune might be a problem when there is no transmission line of the kHz-cavity near a transmission line of the Hz-cavity, as the wavelength of the laser has to be on resonance with a transmission line to lock to it. Still, this setup provides

[5] For more information on Zerodur, see http://en.wikipedia.org/wiki/Zerodur.

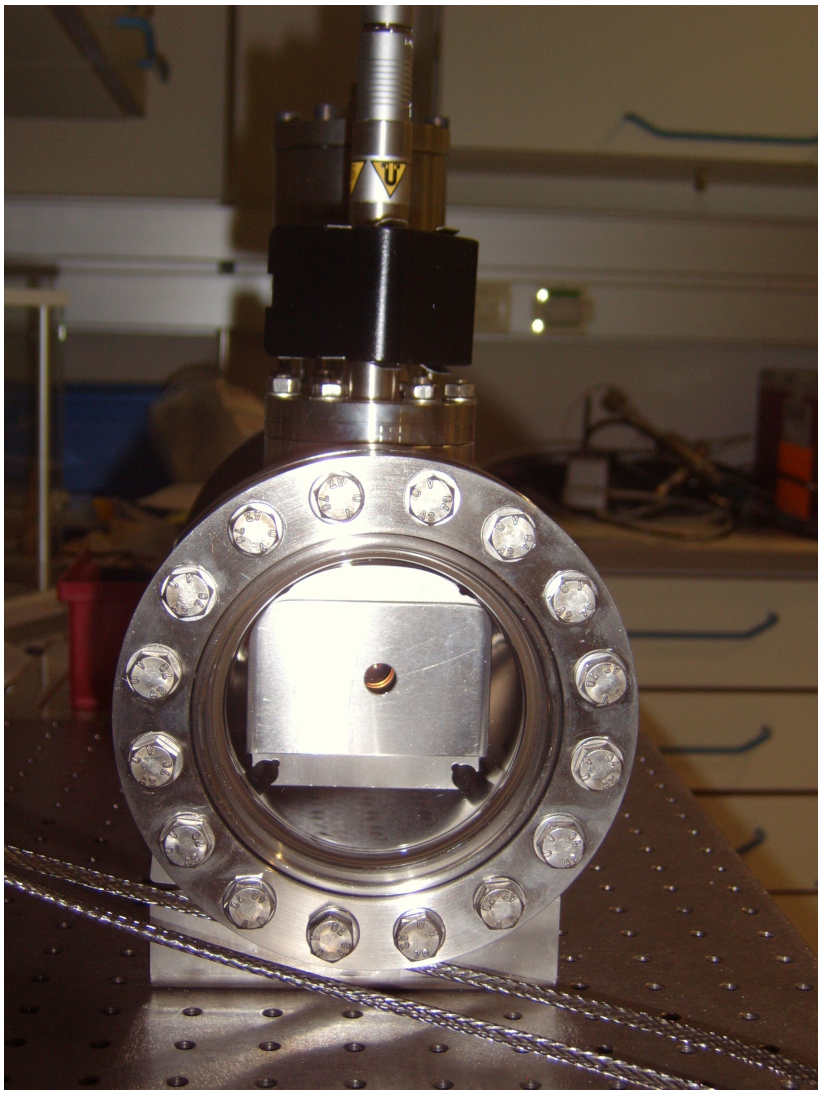

Figure 3.10: Photograph of the vacuum chamber with cavity mounted inside the steelblock through viton rods and protected by radiation shields.

very good stability properties and is a good choice when one only needs good frequency stability without the possibility to tune the absolute frequency of the laser. In the course of this work, one cavity without piezo was built but later replaced by a cavity with piezo.

For our experiment we prefer the possibility to tune one of the transmission lines of the kHz-cavity near to a mode of the Hz-cavity. This is achieved by piezo crystals, between the spacer and the mirrors as seen in figure 3.5. The piezos are made by Annon Piezo and lead to a tunability of several free spectral ranges (1 GHz), when applying up to 200 V.

As the piezo has a temperature expansion coefficient that is orders of magnitude higher than that of Zerodur, the direct use of a piezo between the mirror and the spacer would destroy the good temperature stability achieved through the use of the Zerodur spacer. This is why we use two piezo rings in the configuration shown in figure 3.5, which leads to the expansion of the piezo crystals cancelling each other out to first order. It also reduces the needed voltage needed for a certain change in effective length of the cavity by half.

The connection parts are made from Macor, a synthetic, machinable material and is therefore workable in our own workshop. Macor is also one of the few synthetic materials suitable for vacuum applications due to its low outgassing rate and has a relatively low TEC of $\approx 10^{-5}\,\mathrm{L}^{-1}$. As this CTE is still pretty high compared to the spacer, even when considering that the spacer is much longer, we need to apply the same compensating arrangement as in case of the piezo crystals. As a voltage has to be applied to both piezo rings, there is an additional slit in the outer Macor ring to allow room for the required four wires.

The mirror itself is glued to the outside of the inner Macor ring, which means that the inherent expansion of the mirror material will not affect the cavity length, as the mirror can freely expand to the outside. The same holds for the mirror directly glued to the spacer. Through this setup we manage to keep the temperature stability very high, even though we are using materials with CTEs of magnitudes higher than that of the Zerodur spacer.

We mount the cavity inside a stainless steelblock (see figures 3.6 and 3.9) with dimensions of 47 mm x 470 mm x 175 mm with the help of viton rods. The steelblock acts as a big thermal mass while the mounting on viton rods acts as vibration isolation. Even though Viton is a synthetic material its outgassing rates are comparably low and suitable for our application.

The vacuum chamber consists of a custom made CF100 tube with optical windows at both ends and two CF40 flanges and one CF60 flange welded on top of it (see figure 3.7). It rests on custom made pieces of steel (see figure 3.9, which feature meander-like parts. This design limits the possible heat transfer through its narrow crosssection and provides some vibration isolation, because the configuration gets weakened slightly thus decreasing the stiffness and acting more like a spring than a perfectly stiff material.

The black-body radiation shields, seen in figure 3.8, just consists of 2.5 mm thick aluminum, bend to an U shape, which gets fixed to the steelblock at 4 points, to prevent air resevoirs, which could arise when directly clamping the flat surface of the U-shield to the steelblock.

The used valve is a "Ganzmetall Eckventil" from VAT and we use standard electrical feed-throughs by VACOM and MDC Caburn. The ion pump used are 2 l/s ion pumps from Varian, which is easily enough for our requirements.

For additional thermal insulation we plan to cover the whole setup in

Armaflex foam and built a wooden box around the cavity to shield it from acoustic noise and to provide additional temperature buffer. The box is built from MDF wood, which is also used in the construction of loudspeakers and subwoofers. The box is glued with standard wood cement and lined with acoustic dampening material also used in sound studios.

One can also setup a temperature control of the vacuum chamber by gluing two 10 kΩ NTC temperature sensors to it and winding wires around it with a total resistance of around 5 Ω. Using a PID-controller one can then control the temperature of the vacuum chamber to keep it even more stable.

Even though the piezo crystals are susceptible to radio-frequency coupling as well as a major source of outgassing and drifts, we have not found any significant difference in stability compared to the cavity without piezo. The system even stays relatively stable over some seconds when not locked in any way, and does not get disturbed by acoustic noise or mechanical vibrations in any major way.

3.5.2 Assembly instructions for the kHz-cavity

The step-by-step assembly instructions are as follows: First all of the parts are cleaned with a vacuum cleaning routine. Usually this involves cleaning the parts with rinsing agent, ethanol, methanol and isopropanol. We have found, that for achieving a vacuum on the order of 10^{-6} mbar, it is sufficient to clean every part with isopropanol.

One then solders two vacuum suitable Kapton wires to the inside and outside of each piezo ring. For this all the ends of the wires have to be uncoated and arranged on the same side, so they can all be fed through the slit in the outer macor ring later.

Then one prepares the epoxy by mixing the both ingredients according to the instructions in the data sheet and applies it to the spacer in the form of small droplets. To harden the glue we heat the parts to 80 °C for 30 minutes. While higher temperatures allow for a faster hardening of the glue, one has to be careful, because the mirror coatings are very susceptible to higher temperatures, depending on the original manufacturing process. If possible one should provide some kind of ventilation when gluing the mirrors, as the vapors from the glue can otherwise coat the mirror and degrade its reflectivity. Additionally one should apply gentle pressure when gluing parts, to prevent air bubbles, that can degrade the vacuum, and excessive amounts of glue, which can lead to misalignment.

The viton rods are cut into cylinders with a length of around $3 - 4$ cm and baked at a temperature of 175 °C for around four hours. Through this, the viton loses a lot of water, which would destroy the vacuum. The rods also get thinner, which has to be accounted for, when choosing the thickness of the viton rods.

The whole vacuum chamber, including the ion pump, the feed-through,

the stainless steel block and the blackbody shields, is assembled and pumped down by using a Varian TPS compact (oil-free pre-pump and turbo-pump), then baked for three days using heating wires. As the maximum temperature is quite different for the different parts of the chamber, one has to take care to measure the temperature at all critical points. The pressure reaches 10^{-5} mbar after a few minutes, while it takes around $1-2$ days to reach a pressure of $1-5\times10^{-7}$ mbar. It is also advisable to turn on the ion pump for a short amount of time to get rid of impurities. When doing this, one usually measures a small increase in pressure, followed by a very rapid decay to the original pressure in a few seconds.

The cavity is put inside the clean, stainless steelblock and fixed there by squeezing viton rods into the gaps. Next, the four wires, coming from the piezos, are connected to the electrical feed-through, either by soldering or by using vacuum suitable luster terminals. It should be documented, which wire goes where, as this will be important when applying the voltage to control the piezo.

To couple the laser into the cavity, we first couple a laser pointer, with a wavelength the mirrors are transparent for, into the fiber going to the kHz-stage (also coupling to a separate fiber and switching at the collimators works). As the mirrors are not reflecting at this wavelength, we can find the approximate position of the optical axis very easily. One also can find the position for the photodiode and lens behind the cavity. We then turn off the laser pointer and use the laser light, for which the mirrors are reflective. The back-reflection of the laser light from the mirrors is used to align the two coupling mirrors by lining up the back-reflections (which can be distinguished by their size) with the incoming beam. As this point one usually can already see modes at the camera or photodiode, when the laser's wavelength is scanned. As soon as a signal has been achieved, it can be optimized to a single mode, using mode-matching techniques (see Sec 2.6.4).

3.5.3 Experimental results for the kHz-cavity

In this section we present some measurements to characterize the kHz-cavity. Notice that these are typical measurements and by no means the boundaries of the system's performance. At this point it is unclear, what optimization of the kHz-lock will lead to the best performance of the Hz-lock.

Figure 3.11 shows pictures of three low-order modes of the kHz-cavity. The laser was locked to the respective mode and the signal from the camera, picking up the light transmitted through the cavity, was photographed from a television screen. Figure 3.12 shows the intensity of light transmitted through the cavity, when scanning the cavity length. The mode for which the coupling into the cavity was optimized is clearly visible as dominant peaks. The modes near the dominant mode are sufficiently suppressed to not create any problems in the PDH-signal (see also Sec 2.5). From the width of the

Figure 3.11: Photograph of some modes of the kHz-cavity we successfully locked to. The transmitted light from the cavity was filmed by a camera and transmitted to a television screen, where it could be easily photographed when the laser was locked.

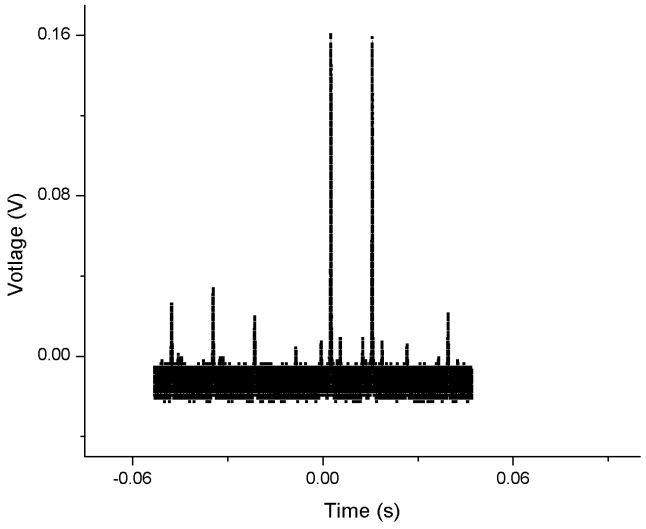

Figure 3.12: Data from an optimized mode of the kHz-cavity. The scanning direction changes between the two high peaks, displaying all modes twice.

peaks one could approximate the finesse of the cavity, but this is better done when sidebands of known distance to carrier can provide a calibration of the time-axis in terms of frequency units.

Figure 3.13 shows a typical measurement of the Pound-Drever-Hall signal, when scanning over a mode. The sidebands' distance to the zero-point of the carrier is the modulation frequency of 71.2 MHz, which was later changed to 34 MHz, see also Sec 3.8. Using this information to calibrate the time axis of the measurement, one can determine a error signal slope of approximately 17 mV/MHz. Notice that this is the error signal measured before the FALC-controller, which offers additional gain directly through its proportional part

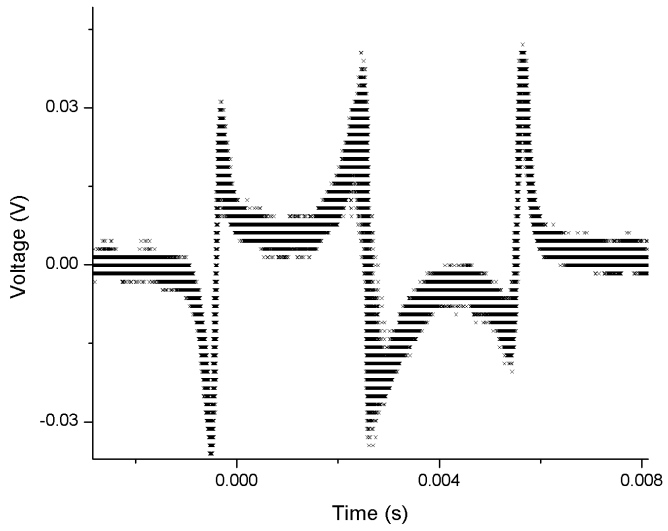

Figure 3.13: Pound-Drever-Hall error signal as it enters the FALC-controller. To measure this data, the laser was scanned over the respective mode using the scan-module. The stripes are digital artifacts created by the oscilloscope.

and frequency-dependent through its integrators [31]. Different modes and the respective PDH error signals are shown in figure 3.14.

As an approximation for the cavity's finesse we measure the width of the transmitted peaks. As discussed in Sec 2.6.2 the arising peak, when scanning the laser over a mode, is a convolution between the Airy function of the cavity's mode and the Voigt form of the laser's linewidth. Figure 3.15 shows a typical measurement of a transmission peak with sidebands at the distance of the modulation frequency of 71 MHz from the carrier. Fitting peaks with a proper function gives information about the width and distances of the peaks. Using the known modulation frequency to calibrate the x-axis, we find a width of about $2\,\mathrm{MHz} \pm 1\,\mathrm{MHz}$. Details depend on the functions fitted (Gauss/Lorentz and Voigt are all good and straight-forward approximations) and the exact definition of width used.

As we are expecting a intrinsic modewidth of around 300 kHz (calculated from the reflectivity of the mirrors and the resulting finesse, see Sec 2.6.1) this points either towards a significant contribution of the laser's linewidth or towards a lower finesse, potentially caused by dirt on the mirrors. As discussed in Sec 2.6.2, it is rather difficult to calculate the laser's linewidth from the finesse and the measured effective width, because one has to work with Airy functions convoluted with the Voigt-profile of the laser, which

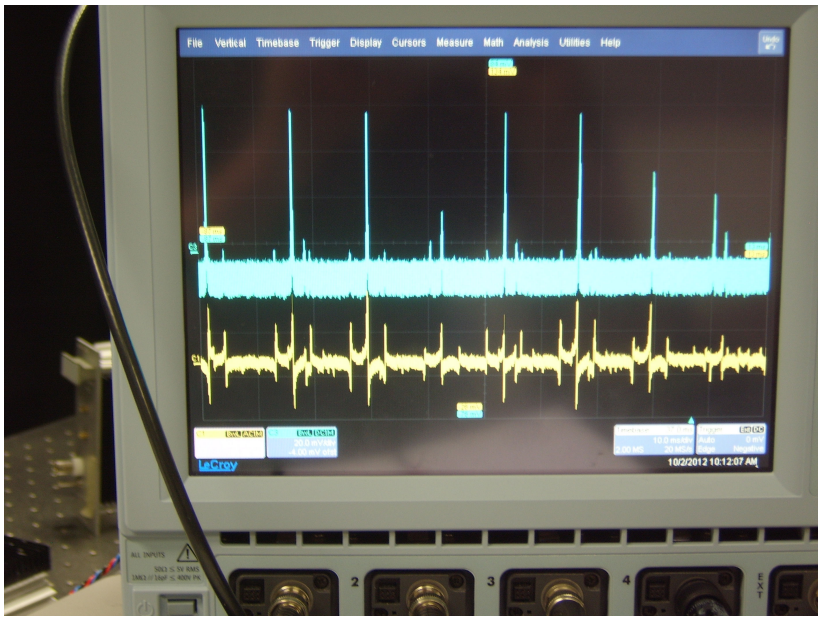

Figure 3.14: This photograph shows the modes of the kHz-cavity, as they are measured by the photodiode behind the cavity, and the corresponding Pound-Drever-Hall error signals as they enter the FALC-controller. This picture was taken after the rf-amplifier had broken, leaving us with not enough power to reach the optimum sideband height of 40% the carrier's height.

is itself a convolution. By using the discussed estimation (see Sec 2.6.2) of assuming Gaussian lineshape for both laser-linewidth and transmission mode-width we find what the laser's linewidth would need to be for the measured data to be consistent. Using Eqn. 2.22 and assuming a width of 300 kHz for the modewidth and the resulting measured effective width of 2 MHz, we find that the laser would have to have a linewidth of 2 MHz to dominate the effective linewidth and explain the measurement.

We also performed the state-of-the-art technique of measuring a cavity's finesse, the so called ring-down measurement. As explained in Sec 2.6.2, the lifetime of the photons inside the cavity is a function of the mirrors' reflectivity and thus of the finesse. We locked the laser to the cavity and closed a mechanical shutter, cutting off the cavity from the laser light. We then monitored how fast the light decayed using the photodiode, measuring the light transmitted through the cavity. Figure 3.16 shows a typical measurement.

As discussed in Sec 2.6.2 the intensity should follow an exponential decay of the form $\exp\frac{-t}{\tau} = \exp -\alpha t$. By taking the logarithm of the measured intensity and performing a linear fit using the program Origin, we find a decay constant $\alpha = 1/\tau = 1.8(3) \times 10^6\,\mathrm{s}$. Using equations 2.25 and 2.21 this gives a linewidth $\Delta\nu$ of 286(45) kHz.

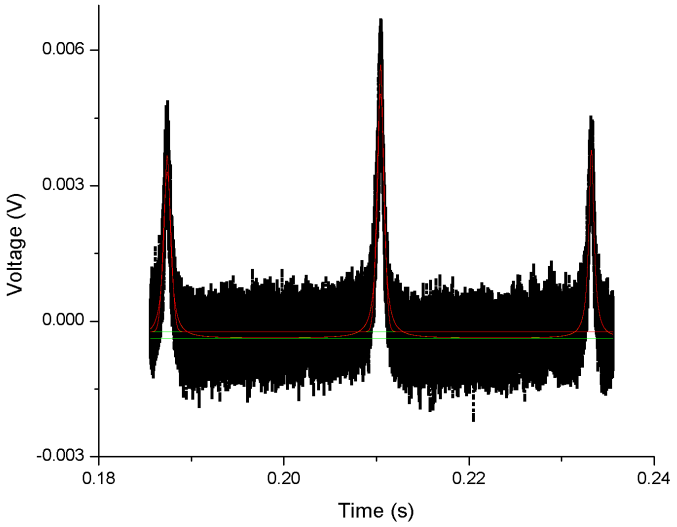

Figure 3.15: An mode of the kHz-cavity with sidebands at a distance of 71 Mhz.

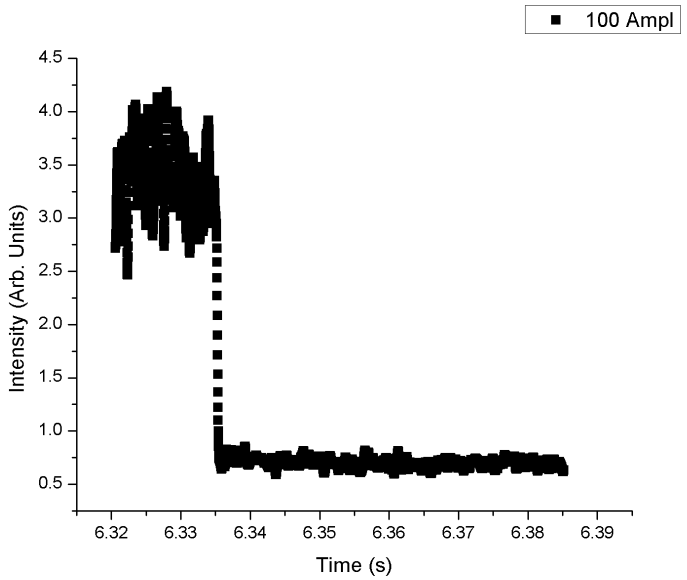

Figure 3.16: Measurement of the decay in the transmitted light through the cavity after locking the laser and closing a mechanical shutter.

	cavity transmission width $\Delta\nu$	finesse
Mirror's Reflectivity	318 kHz	3140
Transmission width	2(1) MHz	500(250)
Ringdown	286(45) kHz	3500(500)

Table 3.5.3 summarizes the results for the finesse from a) direct calculation from the reflectivity of the mirrors, b) measuring the transmission width when scanning the laser over a resonance and c) the ringdown measurement. As was discussed previously, measuring the transmission width when scanning the laser over a transmission peak is problematic, due to the involved mathematical complications. The ringdown measuremt, however, agrees quite well with the predicted value from direct calculation starting from the reflectivity of the mirrors.

3.6 Estimation of the linewidth after the kHz-lock

As discussed in reference [25] it is very difficult to measure the linewidth of a laser below 1 MHz level. While we ultimately plan to measure the linewidth by a beat-measurement with the Hz-laser from Rainer Blatt's group, using a frequency comb to bridge the different wavelength, we here present an estimation of the laser linewidth after the kHz-cavity.

As we can measure the slope of the error signal we are locking to as well as the resulting fluctuations (at the input of the controller) when the laser is locked, we can estimate the laser linewidth. Of course this only includes stability of the laser with respect to the cavity, leaving broadening mechanisms arising through the cavity unmeasured.

The measurements were performed with a modulation frequency of 34 MHz, locking to the TEM10-mode of the kHz-cavity with a laser power of 3 mV incident upon the cavity. Using the methods described in Sec 3.5.3 we measure a error signal slope of 57 mV/MHz. The locked error signal has root-mean-square value of 2.04 mV leading to a lower bound for the linewidth of 17 kHz.

This is just a typical value and the linewidth can be decreased by choosing different settings for the FALC at the cost of long-term stability. At this point it is not clear why those quantities are interrelated in such a way. Using the unlimited integrator from the FALC to cancel out drifts, locking times of one day have been observed, while locking times when optimizing towards smallest possible linewidths are on the order of tens of seconds to minutes.

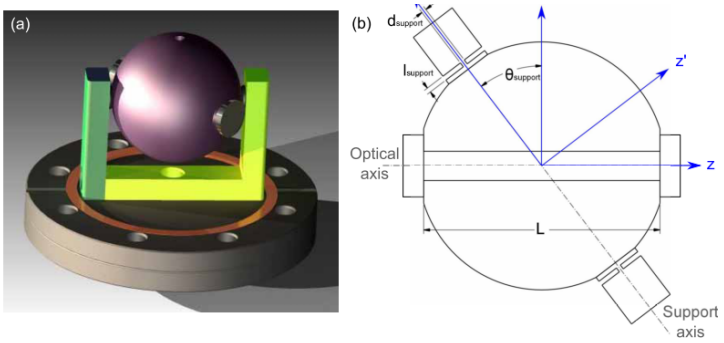

Fig. 1. (a) CAD rendering of a SC mounted at the squeeze insensitive angle with Viton o-ring contacts. Note that this is the experimental design. (b) Cross section of a SC mounted at the squeeze insensitive angle with cylindrical ULE contacts. This is the design used for the finite element analysis model. Important coordinate systems and dimensions are labeled. The sphere is 50.8 mm in diameter and has a 6 mm diameter bore drilled through it along the optical axis. The mirrors are optically contacted to the sphere on flats separated by L = 48.5 mm and are 12.7 mm in diameter and 4.2 mm thick. The two support contacts are attached to the sphere along the support axis which is oriented at $\theta_{support}$ = 37.31° with respect to the y axis and have dimensions $d_{support} = l_{support}$ = 1 mm.

Figure 3.17: Left: CAD-rendering of the spherical-cavity in its mounting (see also figure 3.25) at the squeezing insensitive angle of $\theta = 37.31°$. Right: Sketch of the spherical cavity design, as used in all the simulations in the original proposal. The diameter of the sphere is 50.8 mm and the bore's diameter is 6 mm. The mirrors are optically contacted to flats and are separated by $L = 48.5$ mm from each other. For more information on the model used in the simulations, see the original reference [32]. Figure taken from [32].

3.7 Hz-cavity

As discussed in Sec 2.4 it is very challenging to build a cavity that is sufficiently stable against external influences to reach Hertz levels of stability. While there are a multitude of approaches, this master thesis will only cover the specific realization used in our work. However, we suggest reference [24] as a starting point for interested readers. Much of the information presented here is drawn from [32] and the information from the respective manuals of the products.

3.7.1 Experimental details of the Hz-cavity

The cavity uses a spherical spacer with a diameter of 50.8 mm to hold the cavity, as depicted schematically on the right side of figure 3.17. The high symmetry of this setup serves to minimize the influence of external perturbations, like acceleration sensitivity, on the effective cavity length.

The spacer is made from ultra low expansion glass (ULE) to minimize temperature influence, much like in the case of Zerodur discussed in Sec

Figure 3.18: The spherical spacer, made from ultra low expansion glass, with mounting points at the squeezing insensitive angle of $\theta = 37.31°$ with respect to the optical axis (in front of the left mirror). This makes the ultra high finesse cavity extraordinarily stable against vibrations. Photograph courtesy by Michael Chwalla.

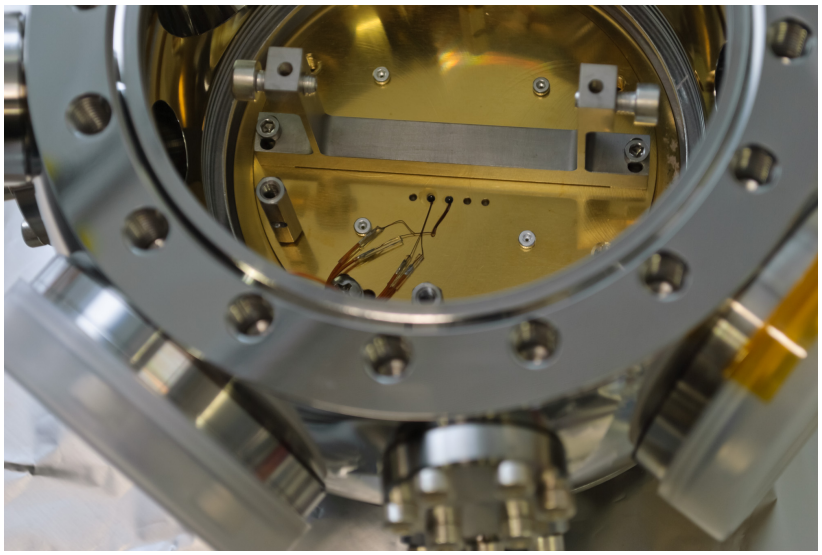

Figure 3.19: The mounting mechanism for the spherical cavity and the wires for the one-point temperature controlling. Photograph courtesy by Michael Chwalla.

3.5. ULE has the useful property that its temperature expansion coefficient vanishes in first order at a certain temperature, usually a point between $5°C$ and $30°C$. This means that stabilizing the cavity to this temperature, which offers advantageous effects by itself, will only leave second and higher order corrections in the thermal expansion behaviour, thereby greatly reducing the sensitivity to temperature fluctuations.

The cavity consists of a spherical mirror, with radii of curvature of 500 mm, and plane mirror. The mirrors are produced by the company AT-Films and are made from fused silica to reduce thermal noise in the mirror substrate, as discussed in reference [33]. ATFilms claims that the cavity has a finesse of approximately 200000-300000, which could not be verified as of yet, because locking to the Hz-cavity has not been achieved for long enough times to perform a ring-down measurement. However, Rainer Blatt's group has already measured the finesse of such a cavity and found a finesse in the given range.

One of the advantages of this setup is its extraordinary insensitivity against accelerations. Even in the prototype version for reference [33] the authors measured acceleration sensitivities as low as $4 \times 10^{-11}\,\mathrm{g}^{-1}$ in the vertical axis and $1.6 - 3.1 \times 10^{-10}\,\mathrm{g}^{-1}$ in the horizontal directions, where $g = 9.81\,\mathrm{m/s^2}$. While many other setups needed high technological effort and investment to achieve this level of vibrations (in)sensitivity, the concept of this spherical cavity is as strikingly simple as it is effective.

The idea is the following: Assume, for the sake of illustration, a horizontal lying cavity inside the spherical spacer as depicted in figure 3.20. Now, some squeezing force, serving as an example for an acceleration caused by some force acting on the spacer, will deform this spacer in some way[6], thereby changing the effective cavity length. As depicted in figure 3.20, squeezing the spacer horizontally will change the effective cavity length in a very direct way by shortening it. On the other hand, squeezing it vertically will flatten the sphere, thus lengthening the effective cavity length. While the effect on the cavity length is diminished in case of the vertical squeezing, by a factor usually called Poisson's ratio, one process lengthens the effective cavity length and the other shortens it. This means that there ought to be an angle of force, respective to the horizontal position of the cavity, where both contributions (horizontal and vertical) on the effective cavity length compensate each other. And indeed, this so called squeezing insensitive angle is found to be $\theta = 37.31°$ with respect to the y axis, as shown in figure 3.17. For more information about the theory behind this and the involved finite element analysis, see reference [33].

Now the idea is that mechanical perturbations, like acoustic or seismic

[6] Actually it is only the difference in force, as applying the same force or acceleration everywhere will not deform the spacer and not change the effective cavity length.

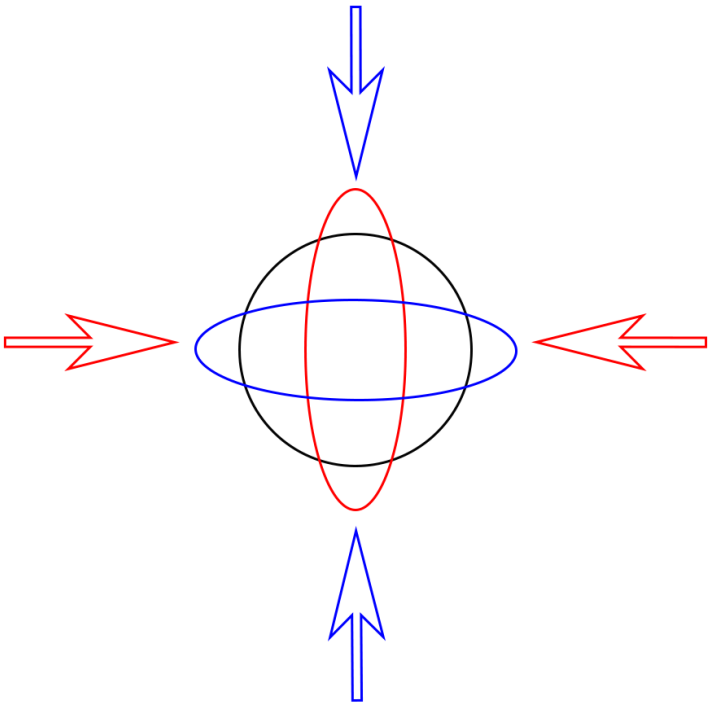

Figure 3.20: When a horizontal squeezing force gets applied to a spherical cavity with horizontal optical axis, it will shorten the effective cavity length. A vertical squeezing force will tend to stretch the effective cavity length (modified by Poisson's ratio).

noise, predominately couple to the cavity through the mounting points[7]. If one mounts the cavity at two points satisfying the squeezing insensitive angle, where the change in length due to the horizontal component of the force and the counteracting change due to the vertical component of the force cancel, the effective cavity length is very stable against acceleration effects.

While there are different possibilities to realize these mounting points, our cavity features small half-spheres at the mounting points, which were supposedly glued or optically contacted to the spacer. Those are then fixed in the mount by two screws applying pressure along the diameter of the sphere, see also Sec 3.7.2.

The Hertz cavity is mounted inside a vacuum can, shown in figure 3.21. This can is produced by Stable Laser Systems and is designed to work with the spherical cavity discussed above. It features one-point temperature sta-

[7] Here we are assuming good vacuum, temperature stability and radiation shielding.

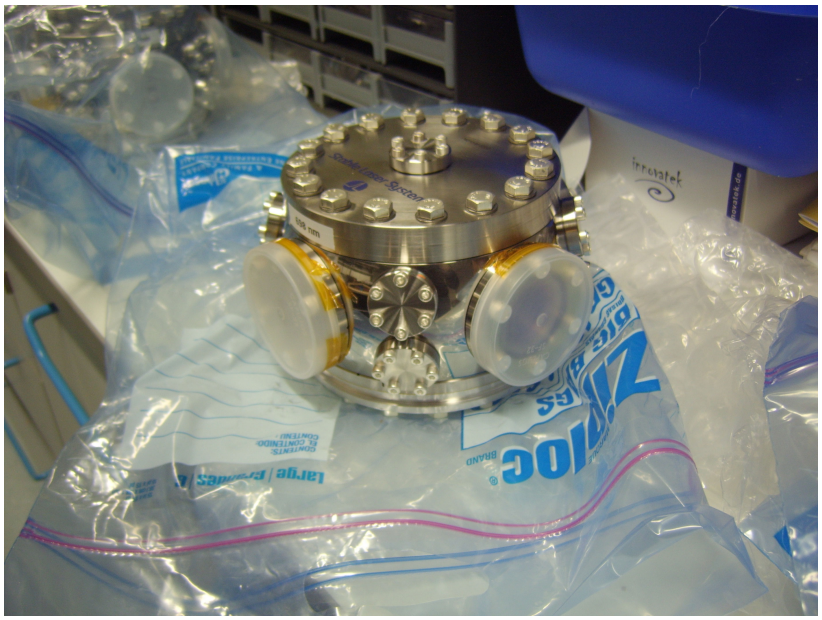

Figure 3.21: The vacuum can with mounting for the spherical Hz-cavity. The vacuum can is one-point temperature stabilized and features radiation shields to protect the cavity from the thermal radiation originating from the ion pump. Photograph courtesy by Michael Chwalla.

bilization to better than 5 mK/°C, which is currently not used, and radiation shielding between the top flange and the cavity (see figure 3.23). We use a Varian 2 l/s ion pump to keep a pressure of less than 10^{-6} mbar.

3.7.2 Assembly instructions for the Hz-cavity

This section offers detailed instructions on how to prepare and assemble the Hertz-cavity for use in the experiment.

First we assembled the vacuum can, using a suitable vacuum T-tube to put a "Ganzmetall Eckventil" from VAT and a 2 l/s-ion pump from Varian on top, see figure 3.22. To pump down the vacuum can, we used an oil-free turbo-pump by Varian. The can is baked at 80 °C, according to the manual, while the ion pump (without magnet), valve and tubes to the pump can be heated to 200 °C. We baked the can for three days, flashing the ion-pump in between, and reached a pressure in the range of 10^{-6} mbar. After a leak test we were confident to have a clean and leak-free vacuum can to proceed.

To mount the cavity inside the vacuum can we worked on a table under a flowbox (HEPA-filter), making sure we would be as quick as possible. After removing the top of the vacuum can, we moved the top of the radiation shield, shown in Fig. 3.24. After removing the protective foil at the bottom of the cavity, seen in figure 3.18, we mounted the cavity, making sure to

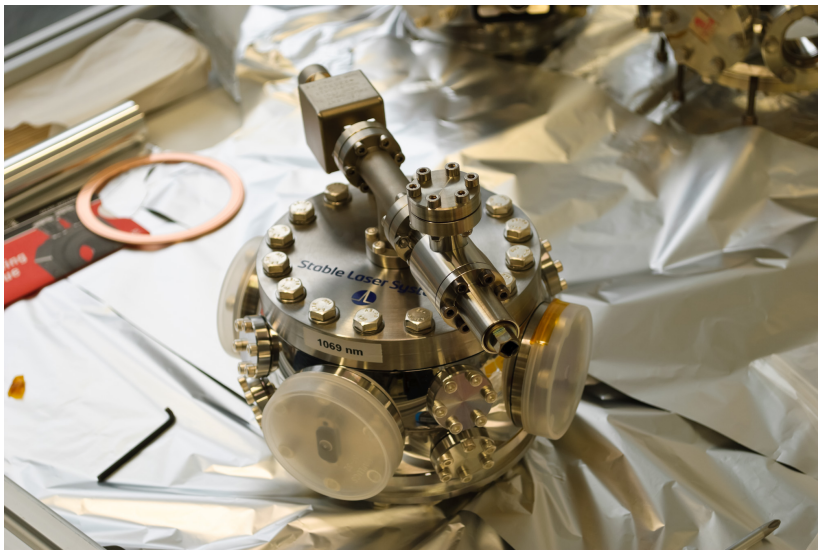

Figure 3.22: The vacuum can for the spherical cavity with a ion pump and valve mounted on top. Notice that our cavity is for a wavelength of 670 nm and 698 nm instead of this one, that is optimized for 1069 nm. Photograph courtesy by Michael Chwalla.

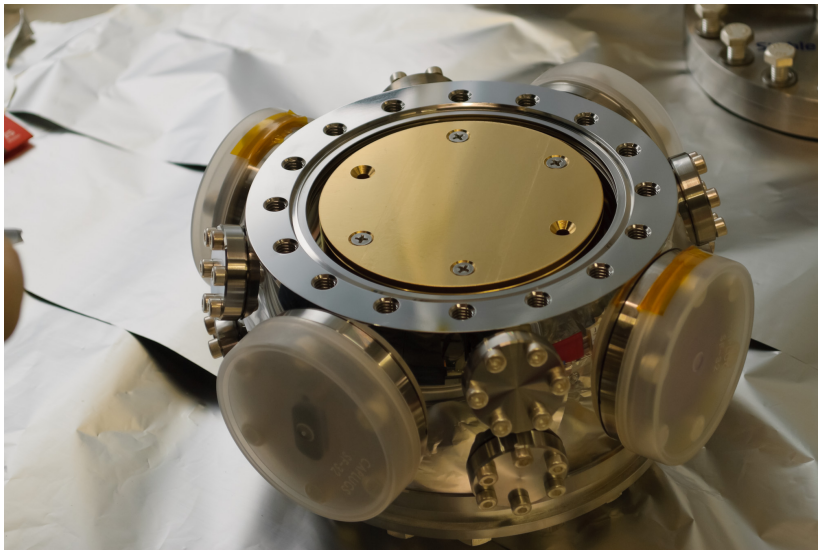

Figure 3.23: The vacuum can for the Hz cavity with the golden radiation shield to separate the cavity from the ion pump that will be mounted on top of the can.

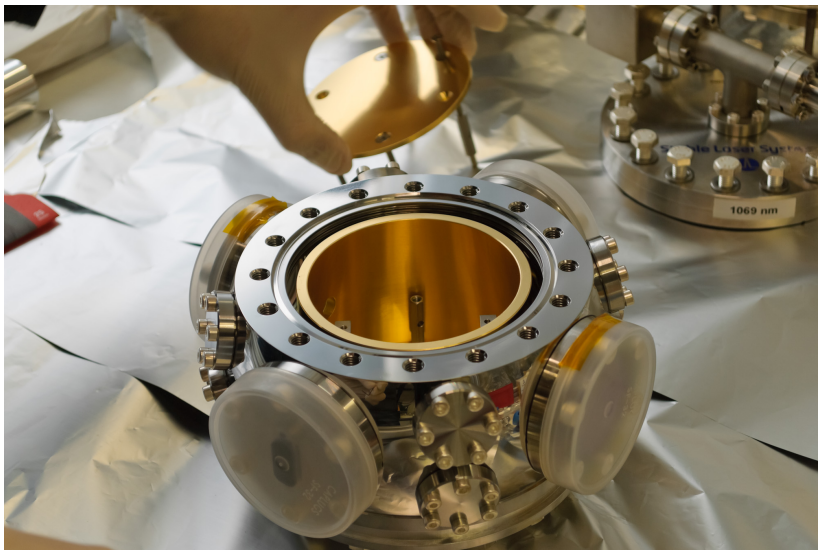

Figure 3.24: Vacuum can with the cover of the radiation shield removed. Photograph courtesy by Michael Chwalla.

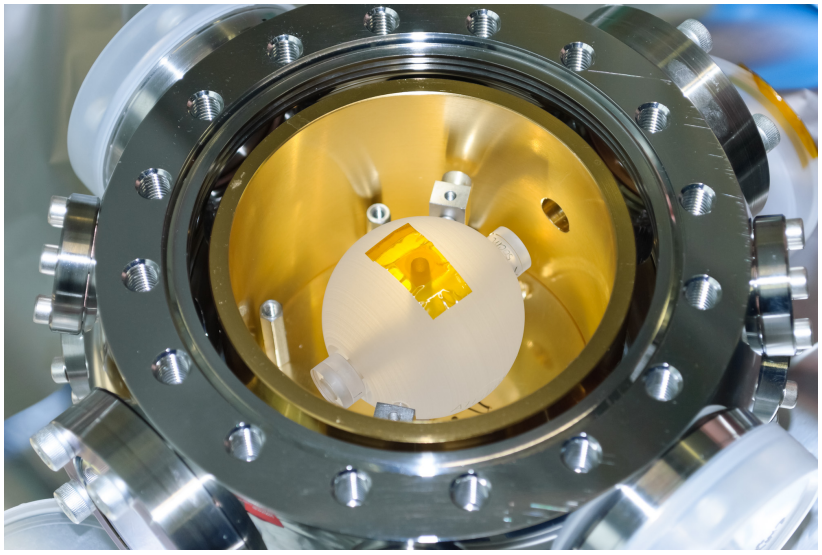

Figure 3.25: The spherical cavity mounted properly after the protecting foil has been removed on the bottom side. Photograph courtesy by Michael Chwalla.

tighten the holding screws equally. Figure 3.25 shows the cavity mounted inside the vacuum can. It is advantageous to note down the position of the different mirrors with respect to the can for later purposes. After removing the second protective coil and checking the alignment of the optical axis with

respect to the vacuum can's windows, we closed the radiation shield, see Fig. 3.23, and the vacuum can.

This time we used a high-performance oil-free turbo-pump station to pump down the vacuum can. First we kept the valve closed, slowly opening it at a pressure of 10^{-4} mbar. The pressure quickly reached a value of 3×10^{-6} mbar. The purpose of this procedure is to prevent any dirt present in the connection tube or pump to get inside the vacuum can. This time no baking was performed, as the maximum temperature for the mirrors is too low to have significant effect.

After two days the pressure was at 1.4×10^{-7} mbar and we flashed the ion pump, which increased the pressure slightly to 3×10^{-7} mbar, turning the pump off again when the pressure had settled back to the pre-flash value. After a leak test we let the pumping continue another day, before performing another leak test and closing the valve. While this procedure might seem overly fastidious, other groups have reported problems with first mounting the cavity inside the can and pumping it down without baking. In one particular instance the mirrors got dirty, degrading the finesse of the cavity to the point, where it had to be sent back to the manufacturer for cleaning purposes.

3.8 Electro-optic modulator

3.8.1 Experimental details for the electro-optic modulator

The electro-optic modulators are used to create the sidebands necessary for the Pound-Drever-Hall stabilization scheme. At the moment both of the EOMs are lithium-niobate crystals, cut at Brewster's angle, in a home made copper housing, as shown in figure 3.26. This casing is made from copper, which is easily machinable, and more resilient against oxidation than other similar materials, like aluminum. Oxidation impairs the electrical conduction between the parts of the housing, thereby potentially derogating shielding. As the housing is also used as ground connection for the electro-optic crystal, it is important to isolate the housing from any connection to the optical table, as this would create a ground loop through the table, housing and the shielding part of the BNC cable.

The signal for the EOM of the kHz-lock is created by a Direct Digital Synthesizer (DDS) system with an amplitude of around -10 dBm and a frequency of 34.1 MHz. For details about the DDS system, see Ref. [34].

Originally we planned to use a modulation frequency of approximately 70 MHz, as a higher modulation frequency increases the capture range of the lock. Following the methods discussed in Sec 2.6.4, we find that the cavity has a approximate mode spacing of around 50 MHz, which means that other modes can lie between the mode one is locking to and its both sidebands. As each mode creates its own PDH error signal of the shape depicted in figure

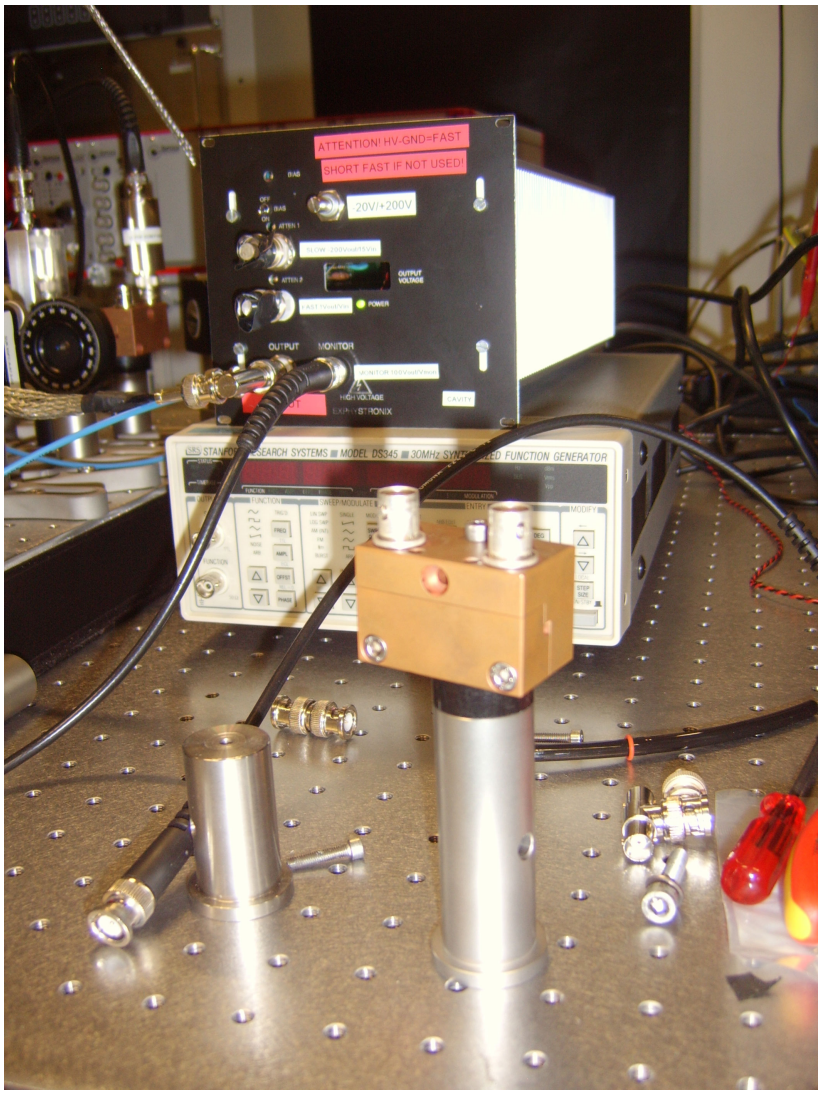

Figure 3.26: Picture of the home-made electro-optic modulator (foreground). On the left side in the far background one can see another EOM with an impedance-matched LC circuit mounted on top, which creates the high voltage needed by the EOM crystal. In the background one can see the high-voltage amplifier for the piezo inside the kHz-cavity (top) and the frequency generator(bottom), creating the 10 MHz clock signal for the Direct Digital Synthesis system.

2.7, this decreases the stability of the lock because every mode leads to an additional zero crossing the laser will lock to, instead of always returning to the zero crossing of the mode we actually want to lock to. As discussed in Sec 2.6.4 other modes can be suppressed by proper mode matching, assuming

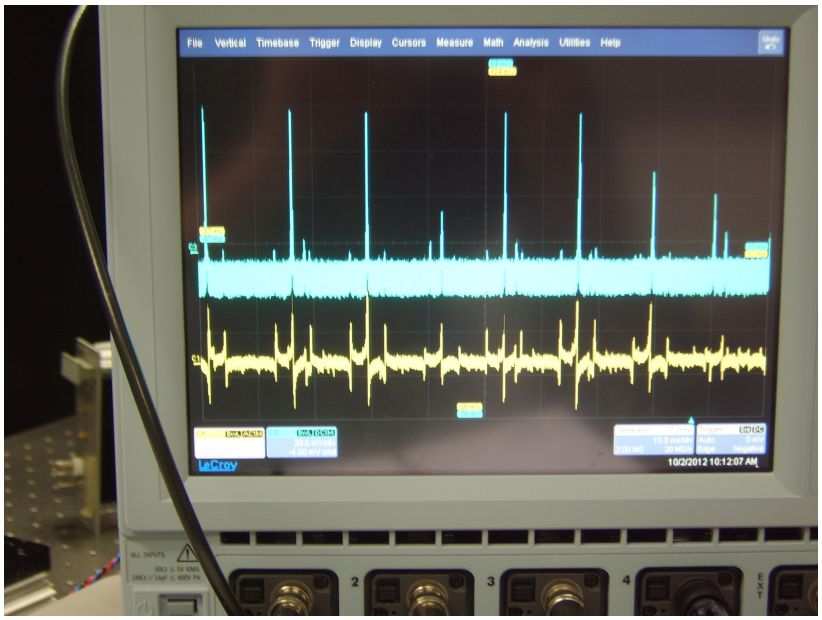

Figure 3.27: The blue channel shows the transmission signal through the cavity, showing the different modes and sidebands of the cavity. The yellow channel shows the Pound-Drever-Hall error signal as it is entering the FALC. This picture was taken, when one of the amplifiers was broken and giving not enough gain to reach the ideal sideband height of around 40% the carrier's height. Still one can see clear zero crossings and sides of the PDH error signal.

the cavity itself is perfect. As neither mode matching (as can be seen from figure 3.12) nor the self-made cavity are perfect we have chosen to change the modulation frequency to 34 MHz. This makes it possible to choose the mode one is locking as free as possible. If one needs to increase the modulation frequency at some point, there are still many modes without residual modes of sufficient strength in vicinity available to lock to.

The 34 MHz signal from the DDS gets amplified by a home-made radio-frequency amplifier, having a gain of about 40 dB. A part of this input signal is used as the local oscillator in the mixer, creating the PDH error signal. When one needs an error signal of higher amplitude, one can use a directional coupler by MiniCircuits, to split off a part of the output signal of the amplifier and use it as the local oscillator. This gives a higher amplitude for the error signal, while the noise properties depend on the specific frequency source and amplifier in use.

The signal from the photodiode, measuring the light reflected at the cavity, is getting amplified by a radiofrequency-amplifier from Mini-Circuits and is mixed with the local oscillator of 34 Mhz to give the PDH error signal. The mixer is a ZFL-500LN-BNC+ circuit by Mini-Circuits. The error signal

is then filtered by a 200 kHz lowpass filter by Mini-Circuits and fed into the FALC[31] by Toptica. An example for the error signal created this way is shown in figure 3.27. The signal from the FALC is then used to modulate the laser current and the grating's position inside the laser, completing the feedback loop and stabilizing the laser.

3.8.2 Assembly instructions for the electro-optic modulator

To assemble the EOM one first has to manufacture the copper housing, which is depicted in figure 3.26. One then mounts two BNC connectors (with connection to the casing) in the respective holes and connects the inner pins by a copper wire without insulation. This has do be done in a way that the BNC connectors are mechanically stable and plugging in cables does not affect the position of the wire inside.

One then cleans the copper with the use of sandpaper to make sure no oxides hinder the electrical conduction. The crystal itself is then clamped carefully between the casing and the wire and, if necessary, additionally fixed with glue. The casing is closed and isolated from the optical table to prevent ground-loops. We are doing this by using a disk of PVC between the casing and the optical mounting post and by insulating the screw from the casing with a layer of insulation tape and a plastic washer.

3.8.3 Suggestions for improving the electro-optic modulator

In this section we present some disadvantages of the current EOM design and offer suggestions for improvement.

The two BNC connectors are bulky and could easily be replaced by one SMA-connector. Instead of clamping the crystal with a wire, one could mill a flume for the crystal to lie in, restricting its movement in one direction. A plate of copper, connected the the casing by plastic screws could then easily hold the crystal in a precisely defined way, while still being isolated from the electrical ground of the casing. Of course, this somewhat restricts the possible sizes of the crystal, so only using the copper plate without a flume could be preferable.

Another flaw of the current design is that the inductance of the LC circuit, needed for creating the high voltage for the EOM, is outside the housing. As the capacity of this resonant circuit is the electro-optic crystal itself high amounts of electric energy is flowing between the crystal and the inductance. Passing through the BNC connectors and increasing distance between those two components lead to losses and makes shielding of radio-frequency emission more difficult. We suggest milling some space into the housing, so the complete LC circuit is inside the copper housing.

3.9 Assembling the LC circuit for the electro-optic modulator

The electro-optic crystal needs voltages higher than 100 V to operate properly. As the DDS gives a maximum output power of −10 dBm, which then gets amplified to 30 dBm by the rf-amplifier (see also Sec 3.8.1), this gives a signal of 20 V peak-to-peak amplitude. We use an impedance matched LC circuit to resonantly amplify the voltage and create the needed high-voltage. The circuit used is shown in figure 3.29.

The capacity of the circuit is the electro-optic-crystal itself, with a capacity on the order of 15 pF. Depending on the modulation frequency needed, we add an inductance of appropriate size. The inductance is a coil without core, handmade from copper wire. Alternatively a high quality commercial inductance can be used. However, a ferrite core would only degrade the quality factor of the core, as the realignment of the dipoles due to the changing electric field of the resonant circuit creates friction, heat and thereby loss of energy.

Impedance matching is crucial for this application, as insufficient matching leads to high amounts of power being reflected at the circuit and coming back to the amplifier. This backreflection leads to overloading of the amplifier's output stage, either continually degrading the amplifier's gain or outright destroying it. For further details concerning impedance matching see reference [35].

3.9.1 Step-by-step instructions for assembling the LC circuit

This section offers details on how to build and impedance match a suitable LC circuit for a given electro-optic modulator, when the target frequency is known. These instructions are based on notes by Meng Khoon Tey.

1. First one measures the capacity of the EOM by taking a commercial inductance and connecting it in series to the EOM. Then one measures the resonance's position with the help of a directional coupler. This device splits off a very small fraction (on the order of 10^{-4} or less) of the signal applied to the INPUT port to the COUPLED port – the main part of the signal appears on the OUTPUT port of the coupler.

   While this is the prime application for the directional coupler, one can also use it as a way to measure reflected signals coming back from a circuit. This is done by sending a sinusoidal signal to the COUPLED port of the coupler, which will appear at the INPUT port of the device, where we connect the circuit. Reflections will come back in at the INPUT port and predominately appear at the OUTPUT port of the coupler, where we connect the measurement device (oscilloscope or measurement part of the network analyzer). Only a small fraction of

Figure 3.28: Reflection of the LC circuit in dependence of the frequency. The resonance is clearly visible, along with two resonances arising from parasitic components.

the reflected signal will appear at the COUPLED port and thus be fed back to the signal generator source.

By sending signals of different frequencies to the circuit and measuring the respective reflection one can directly measure the transfer curve of the circuit [26]. At the resonance frequency of the circuit the amplitude of the reflection will decrease sharply, because the energy will be built up inside and oscillate between the inductance and capacity, enabling us to determine the resonance frequency of the circuit.

By using the equation

$$2\pi f_0 = \omega = \frac{1}{L_0 C_{\mathrm{EOM}}}, \tag{3.2}$$

one can determine the capacity C_{EOM} of the EOM from the resonance frequency f and the known inductance L. The EOM's capacity is typically on the order of $10 - 20\,\mathrm{pF}$.

2. Now that we know the capacity of the EOM crystal, we can wind a coil of inductance L, appropriate to build a LC circuit at the target frequency.

   Using Eqn. 3.2 one can find the needed inductance L from the target resonance frequency f and the capacity C_{EOM} of the EOM, which was

measured in the last step.

The dimensions of the coil in μH can be found by using the following relation

$$L = \frac{(a+2d)^2 \times w^2 \times 0.0393701}{d^2(18 \times (a+2d) + 40 \times w}, \tag{3.3}$$

where a is the inner diameter of the coil in mm, w is the length of the coil in mm and d is the diameter of the wire used in mm. Typical values would be $a = 8\,\text{mm}$, $w = 25\,\text{mm}$ and $d = 1\,\text{mm}$.

3. The self-made coil is now put in series to the EOM (like we did with the commercial coil before), either by creating space inside the copper housing and directly soldering the inductance to the wire going to the EOM or by using an appropriate container with BNC connectors. Now we once again measure the resonance position of the resulting LC circuit with the help of a network analyzer and a directional coupler, as described before. From equation 3.2 we can find the real (the equation only gives us an approximation of course) inductance of the coil we made. If everything was done correctly, the position of the resonance should be near the target resonance frequency.

4. To impedance match the circuit we have first to measure the real resistance of the LC circuit. While inductances and coils usually only have reactances there is always a certain amount of resistance from parasitic effects or just the ohmic resistance of the wires themselves.

   The idea to measure this is the following: We apply a sinusoidal signal with certain amplitude at the resonance frequency and measure the voltage drop at the LC circuit. We basically use the 50 Ohm output resistance of the signal source as one of the two resistances of a voltage divider, with the second resistance the unknown resistance of the LC circuit.

   There is a subtlety involved: When one switches a voltage source to output a voltage (or power level), for example 10 V, the source will actually apply twice the voltage, for example 10 V, internally, because half of the voltage will drop at the output resistance when a proper 50 Ohm impedance load is connected. This means that the voltage of the source, when using the voltage divider picture, is actually twice the voltage shown at the panel of the signal generator.

   So the resistance of the LC circuit can be found from the voltage divider relation

$$V = \frac{2V_0 R}{50\,\Omega + R}, \tag{3.4}$$

   where is the V_0 is the voltage applied (as shown on the display) and V is the voltage measured between entrance point of the LC circuit and ground.

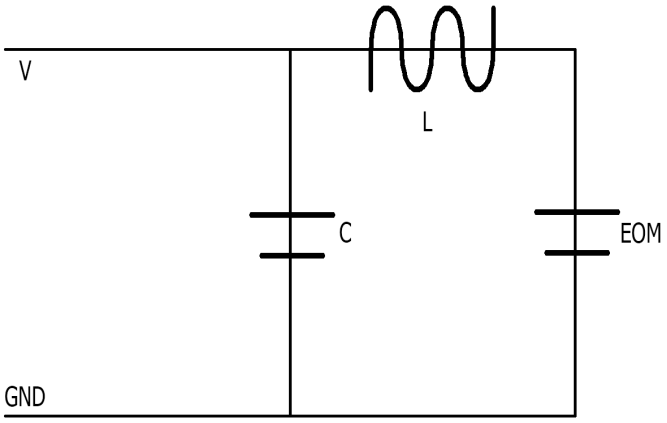

Figure 3.29: Schematic of the LC circuit, consisting of the EOM and the self-made coil, and the additional capacity C for impedance matching.

5. As we now know the inductance L of the coil, the capacity C_{EOM} of the EOM and the resistance R of the total LC circuit, we can calculate the capacities (and inductances, depending on the way the impedance matching is achieved) needed. As shown in figure 3.29, we will achieve mode-matching by inserting an additional capacity of proper dimensions in parallel to the whole LC circuit. This is a practical simplification of the impedance matching presented in reference [35], which is conceptually easier to understand but needs an additional inductance. Following a similar calculation as in reference [35] we can calculate the dimension of the capacity as

$$C = \frac{z + \sqrt{C_{\mathrm{EOM}}(50\,\Omega - R)R(4L + C_{\mathrm{EOM}}50\,\Omega R - CR^2}}{2 \times 50\,\Omega \times R} \qquad (3.5)$$
$$\text{with } z = -C_{\mathrm{EOM}} \times R \times 50\,\Omega + C_{\mathrm{EOM}}R^2.$$

   C_{EOM} is the capacity of the EOM, L the inductance of the self-made coil and R the resistance of the LC circuit before the impedance matching. A typical value for the total capacity C is 245 pF.

   As this is only an approximate value we split the capacity for impedance matching into a fixed value capacity and a tunable capacity. As capacities in parallel add, we now have the LC circuit and the two impedance matching capacities parallel to it (making up the effective capacity C,

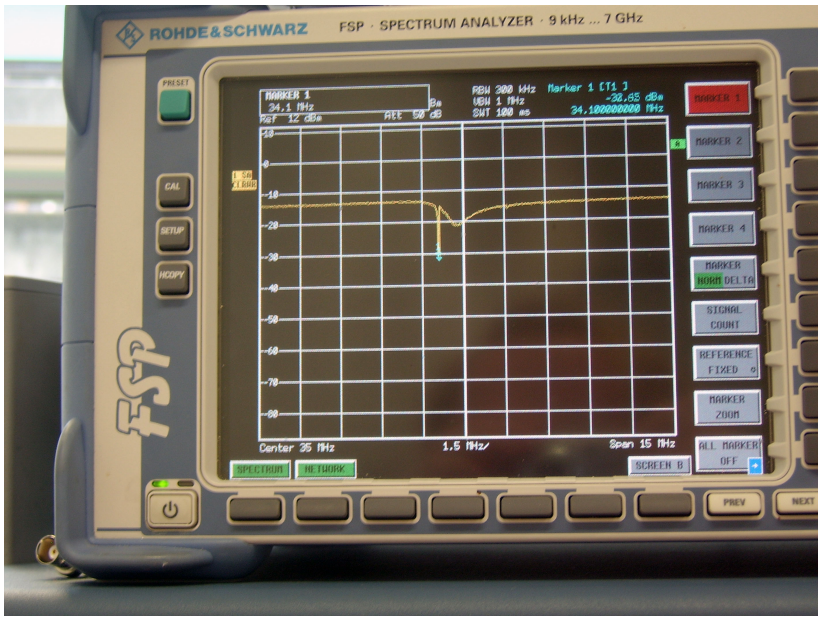

Figure 3.30: Reflection of the impedance-matched LC circuit in dependence of the frequency. Notice how the resonance dip is lower by orders of magnitude compared to the initial value.

also in parallel). One then adjust the tunable capacity to the value, where the amount of energy getting reflected is the lowest(as impedance matching corresponds to the maximum amount of energy transferred from the source to the circuit and thus minimizing the reflected power). Figure 3.30 shows a typical example for this step.

6. A problem arising in impedance matching the EOM-circuit, is that need for measuring voltages and tuning the capacity forces part of the impedance matching to be done without any shielding around the circuit. This can allow stray radiofrequency to distort the measurement but more importantly the shielding is a parasitic capacity, distorting the resonance frequency of the circuit and thereby distorting the measurements. For example, we soldered the inductance and the matching capacities into a small shielding box, connected to the EOM by BNC.

   Figure 3.31 shows how the remounting of the casing changed the behaviour of the LC circuit, basically making the impedance-matching obsolete. While one can optimize the tunable capacity to the lowest resonance WITH the shielding in place, it is usually too much to compensate for (the fixed part of the capacity, determined through measurements without shielding, is too far away from the required value). Apart from using an other impedance-matching technique, this prob-

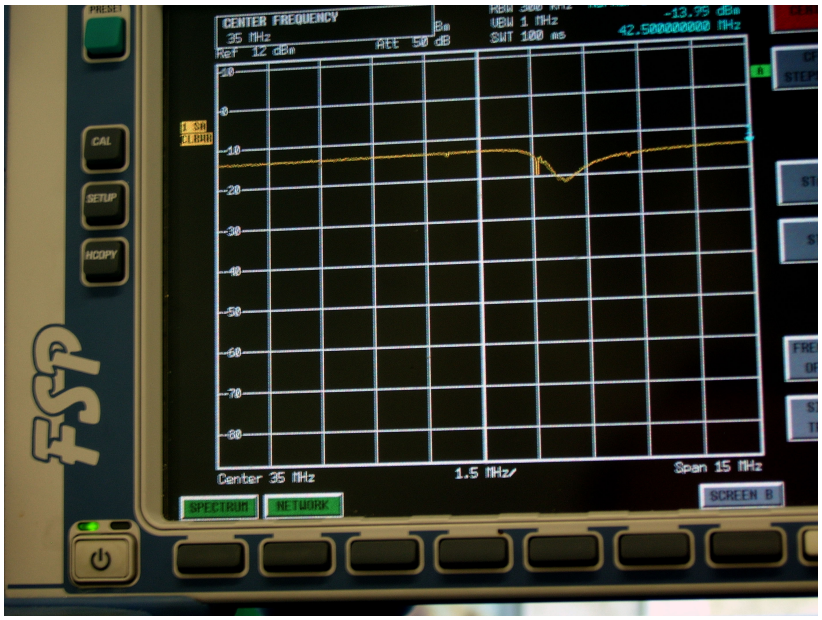

Figure 3.31: Reflection of the impedance-matched LC circuit after remounting the shielding in dependence of the frequency. Notice how the resonance dip is shifted compared to figure 3.30 destroying the impedance-matching.

lem can be resolved by using a shielding farther away from the circuit, giving a smaller parasitic capacity, thus decreasing the impact on the circuit. Maybe it would also be possible to use two tunable capacities, one on the the order of the fixed capacity and one for fine tuning. Then one could optimize the impedance-matching of the circuit to the lowest resonance in the reflection by changing both capacities through two small holes in the shielding.

Note that the shielding is very important as an unshielded LC circuit will act as an antenna and emit huge amounts of radio-frequency waves into the setup/laboratory. Also, radio-frequency can couple to the LC circuit and thus to the modulation of the light, creating additional noise and potential problems.

3.10 Vibration isolation system and breadboards

The whole setup rests on two honeycomb breadboards, allowing for easy transportation from the preparation laboratory to the laboratory in which the Strontium experiment is located. While the kHz-stage rests on a steel breadboard, made by Newport, for increased rigidity, the Hz-stage is mounted on an aluminum breadboard by Thorlabs. Sufficient rigidity is a crucial factor in choosing the breadboards, because otherwise optical alignment may

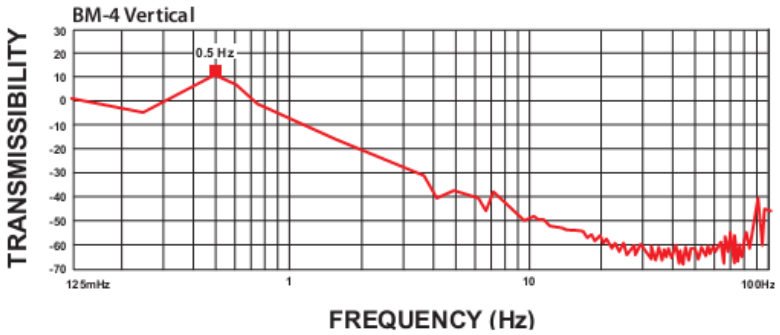

Figure 3.32: Typical performance of a BM-4 vibration isolation platform by minus-k technology. It shows how strong a vibration of certain frequency is transmitted to the load, in units of decibel. At resonance frequency there is a very strong response, while vibrations of higher frequency are suppressed strongly. Figure taken from the BM-4 datasheet.

change, due to changes made (for example, tightening a screw) on another part of the board. We have chosen aluminum for the Hz-stage because we are planning to use a commercial vibration isolation platform to further decouple the setup (especially the Hz-cavity) from seismic vibrations. According to the manufacturer the platform offers 10-100 times better isolation than the air-based optical tables.

While achieving 10 Hz linewidth should be possible without the platform, due to the vibration insensitivity of the Hz-cavity (see Sec 3.7, the platform should allow us to push the performance of the setup to even lower linewidths.

The idea is to create a system with vanishing stiffness, so vibrations do not couple to the load. On the other hand the platform needs to be able to support weight, which needs a certain amount of stiffness. The vibration isolation platform uses so called negative-stiffness mechanisms to decrease the stiffness of the platform without compromising its load capacity. For more details, see [36].

We have chosen a BM-4 passive vibration isolation platform by the company minus-k technology. This model offers resonance frequency as low as $0.5 - 1$ Hz, which means that vibrations of higher frequency will only couple inefficiently to the load, see figure 3.32. The choice of the model and its performance depend on the load, so the weight has to be approximated beforehand. This is also the reason we are using a aluminum breadboard for the Hz-stage, simply because it is lighter.

Details on the performance of the isolation platform and further information can be found in [37].

3.11 Fiber stabilization

Once a linewidth of less than 1 kHz has been achieved, it is important to frequency stabilize the optical fibers guiding the light to the experiment. Otherwise the linewidth will be broadened to the order of kHz, due to strain and temperature variations along the fiber.

We plan to stabilize the fiber in the following way: Using a polarizing beam splitter we split off some of the incident light, while sending the transmitted light through an AOM, operated at 80 MHz, and a $\frac{\lambda}{4}$-waveplate. By using a fiber, polished at zero degree angle, at the output, we make sure that a small part of light is reflected there. This light is returning through the fiber, passing the waveplate and AOM (picking up another 80 MHz like in a double-pass configuration) and gets superimposed with the light we split off at the first pass. This means that the incoming light and the reflected ligth, shifted by 160 MHz plus noise, beat at the photodiode. By stabilizing the beat frequency to 160 MHz, using the AOM as an actuator through a voltage-controlled-oscillator, one can cancel the noise from the fiber. As the Blatt group already has a printed circuit design for these frequencies, we ordered the appropiate voltage-controlled-oscillators (VCOs) from Micronetics. We also ordered some newer products, which haven even better phase-noise properties, which may offer even better performance at only minimal changes to the printed circuit design.

Chapter 4

Current status of the project and outlook

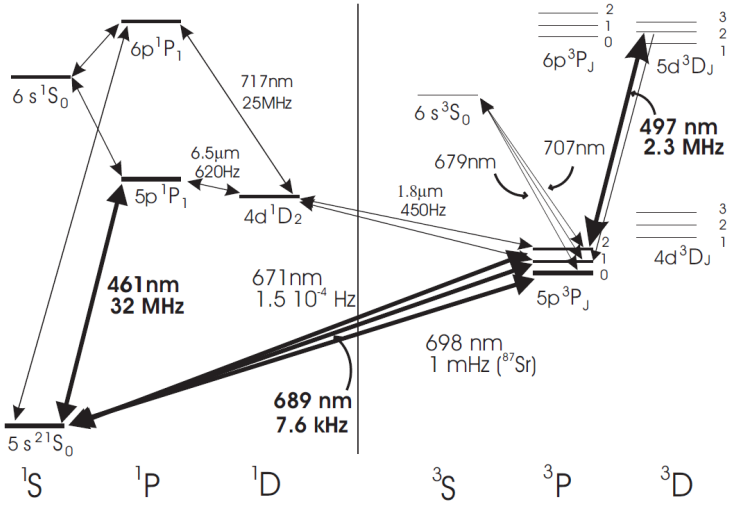

Figure 4.1: Schematic of some states and transitions of Strontium. The clocklaser presented in this work, will work on the 5^1S_0 and 5^3P_0-transition with a wavelength of 698 nm. Figure taken from [10].

The laser can be locked to the kHz-cavity, achieving locking times exceeding one day. It seems that improving the stability of the lock increases the linewidth of the laser, which can be approximated by the variance of the error signal when locked. As the mode we are locking to has a linewidth of around 300 kHz and the control systems can stabilize the laser's frequency to at least 1/10-th of this value (rules of thumb vary between a factor of 1/100 and 1/1000), the locked laser should have an estimated linewidth of around 20 kHz after the kHz-lock, with broader linewidths increasing stability of the lock.

By using the piezo of the resonator, the position of the mode can be varied over more than the free spectral range of the Hz-cavity.

The DDS-system can be used to control the intensities and modulation frequencies of the two EOMs creating the sidebands for the two locking stages.

The infrastructure and optical setup for the Hz-cavity has been done. We directly locked to the Hz-stage for about 30 s, using the infrastructure of the kHz-cavity. Locking to the Hz-cavity using the two-stage setup has not yet been achieved. The question, if using the acousto-optic-modulator as actuator through the external modulation input of the driving signal generator works for locking, is still open.

The 40 m fiber and the parts for the fiber stabilization have been purchased.

In this section we will give an overview over some possibilities for the experiments that can be performed using the Strontium machine and the

clock laser. Most of the experiments can also be performed with other class II elements, like ytterbium or magnesium. As of yet it is still unclear, which systems will provide most suitable for certain applications.

Many of the possibilities, when working with Strontium, arise through the special singlet-triplet level structure, which are shown in figure 4.1. These states of course arise from the fact that Strontium is a group II element in the periodic table and has two electrons in its outermost electron shell. The indistinguishability of the electrons leads to a formation of singlet- and triplet-states, like in H_2-molecules or He-atoms – cases which are often discussed in textbooks, for example [38].

As dipole interactions, which are usually the dominant effects in light-matter interactions, do not involve spin, there is no dipole coupling between singlet- and triplet-states. While transition are still allowed through other, weaker mechanisms [10], the coupling strengths are weak compared to the dipole transitions and thus the arising lines a very narrow. For example, the 5^1S_0 - 5^3P_1 transition, which is used for narrow-line laser cooling and in the red magneto-optical trap, has only a linewidth of 7.4 kHz. The transitions 5^1S_0 - 5^3P_0 and 5^1S_0 – 5^3P_2 have even narrower linewidths, in the sub-Hz range.

The clock transition 5^1S_0 - 5^3P_0 is currently used to build optical clocks, reaching a stability of 10^{-17} ($\tau = 10^3$ s), far outperforming the current standard Cs-based clocks and rivaling ion-clocks. More information on optical clocks can be found in reference [39].

Another interesting aspect of Strontium is that the 5^3P_0 has no total angular momentum $J = 0$, which means it is very stable versus magnetic field influences. This fact also means that the nuclear spin ($I = 0$ for the bosonic isotopes and $I = 9/2$ for the fermionic isotope of Strontium) can be decoupled from the electronic spins in this state [40, 41]. This insensitivity to external perturbations makes Strontium (and other class II elements) attractive candidates for quantum computation, with the ground-states and clockstates as qubits [7].

Using the nuclear spin as one or multiple qubits has also been proposed, see for example section two in [9]. This scheme has the advantage that the qubit(s) are stored in the nuclear spin while the electronic states can be used for manipulation (e.g. gates). The decoupling of the nuclear spin from the electronic configuration (in some states) also offers the possibility to research SU(N)-phenomena, with N being the number of nuclear spin states. This allows for quantum simulation up to SU(10) in the case of the fermionic ^{87}Sr, which has a nuclear spin of $I = 9/2$ [42].

The generation of optical flux lattices is another very interesting experiment, which has been proposed for Strontium using a clock laser [12]. With this technique one should be able to simulate the influence of magnetic fields

on charged particles, using neutral atoms[1]. While this is interesting in its own right, successful implementation of such artificial gauge fields, which are expected to be much stronger than other techniques applied so far, could lead to a whole new array of possible experiments, for example the exploration of the quantum Hall effect.

A review about the possibilities these elements offer and the states of the art in terms of experimental techniques can be found in reference [9].

[1] For more information on the advantages of using neutral atoms in simulation and clock experiments see for example reference [43].

Bibliography

[1] *Laser Technology*, C. Xinju, 2nd ed. (CRC Press, New York, 2010).

[2] *Making Optical Atomic Clocks More Stable with* 10^{-16}*-level Laser Stabilization*, Y. Y. Jiang, A. Ludlow, N. D. Lemke, R. W. Fox, J. A. Sherman, L.-S. Ma, and C. W. Oates, Nature Photon. **5**, 158 (2011).

[3] *Visible Lasers with Subhertz Linewidths*, B. C. Young, F. C. Cruz, W. M. Itano, and J. C. Bergquist, Phys. Rev. Lett. **82**, 3799 (1999).

[4] *Frequency Comparison of Two High-accuracy* Al^+ *Optical Clocks*, C. W. Chou, D. B. Hume, J. C. J. Koelemeij, D. J. Wineland, and T. Rosenband, Phys. Rev. Lett. **104**, 070802 (2010).

[5] *Providing* 10^{-16} *Short-term Stability of a 1.5 μm Laser to Optical Clocks*, C. Hagemann, C. Grebing, T. Kessler, S. Falke, C. Lisdat, H. Schnatz, F. Riehle, and U. Sterr, IEEE Trans. Instrum. Meas. **99**, 1 (2012), arXiv:1208.1634 .

[6] *Prospects for application of ultracold* Sr_2 *molecules in precision measurements*, S. Kotochigova, T. Zelevinsky, and J. Ye, Phys. Rev. A **79**, 012504 (2009).

[7] *Quantum Computing with Alkaline-Earth-Metal Atoms*, A. J. Daley, M. M. Boyd, J. Ye, and P. Zoller, Phys. Rev. Lett. **101**, 170504 (2008).

[8] *Optical Flux Lattices for Ultracold Atomic Gases*, N. R. Cooper, Phys. Rev. Lett. **106**, 175301 (2011).

[9] *Quantum computing and quantum simulation with group-II atoms*, A. J. Daley, Quantum Inf. Process. **10**, 865 (2011).

[10] *Cooling of Sr to High Phase-Space Density by Laser and Sympathetic Cooling in Isotopic Mixtures*, G. Ferrari, R. E. Drullinger, N. Poli, F. Sorrentino, and G. M. Tino, Phys. Rev. A **73**, 023408 (2006).

[11] *The Strontium Optical Lattice Clock: Optical Spectroscopy with Subhertz Accuracy*, A. Ludlow (PHD-thesis) (University of Colorado at Boulder, 2008).

[12] *Optical Flux Lattices for Ultracold Atomic Gases*, N. R. Cooper, Phys. Rev. Lett. **106**, 175301 (2011).

[13] *Frequency Comparison of Optical Lattice Clocks beyond the Dick Limit*, M. Takamoto, T. Takano, and H. Katori, Nature Photon. **5**, 288 (2011).

[14] *Strontium and Mercury of Optical Lattice Clocks*, S. Bize in *Laser Science* (Optical Society of America, 2012) p. LW1I.2.

[15] *Electronic Frequency Stabilization of Microwave Oscillators*, R. V. Pound, Rev. Sci. Inst. **17**, 490 (1946).

[16] *Laser Phase and Frequency Stabilization Using an Optical Resonator*, R. W. P. Drever, J. L. Hall, F. V. Kowalski, J. Hough, G. M. Ford, A. J. Munley, and H. Ward, Appl. Phys. B. **31**, 97 (1983).

[17] *Gerthsen Physik*, D. Meschede, 23rd ed. (Springer-Verlag Berlin Heidelberg, 2005).

[18] *Fundamentals of photonics*, B. E. A. Saleh and M. C. Teich (Wiley, New York, 1991).

[19] *Experimentalphysik 3*, W. Demtröder (Springer-Verlag Berlin Heidelberg, 2009).

[20] *Laser physics*, M. Sargent III, M. O. Scully, and W. E. Lamb Jr. (Westview Press, Boulder, Colorado, 1974).

[21] *Using diode lasers for atomic physics*, C. E. Wieman and L. Hollberg, Rev. Sci. Inst. **62**, 1 (1991).

[22] *Introduction to Solid State Physics*, C. Kittel, 6th ed. (John Wiley & Sons, Inc., New York, 1986).

[23] *Solid State Physics*, N. Ashcroft and N. Mermin (Saunders College, Philadelphia, 1976).

[24] *Optical Coatings and Thermal Noise in Precision Measurement*, M. J. Martin and J. Ye, in *Optical Coatings and Thermal Noise in Precision Measurement*, edited by G. Garry, T. Bodiya, and R. DeSalvo (Cambride University Press, 2011).

[25] *OSA Handbook*, J. Hall, M. Taubman, and J. Ye in *OSA Handbook, 13th edition* (The Optical Society, 1999).

[26] *Feedback for physicists: A tutorial essay on control*, J. Bechhoefer, Rev. Mod. Phys. **77**, 783 (2005).

[27] *An Introduction to Pound-Drever-Hall Laser Frequency Stabilization*, E. D. Black, Phys. Rev. Lett. **69**, 79 (2001).

[28] *DL pro - Grating Stabilized Diode Laser Head Manual*, Toptica Photonics AG, (2011).

[29] *Circularize an Elliptical Laser Beam*, HoloWiki Community, URL: http://www.holowiki.com/ (2012).

[30] *Linewidth Reduction of a Diode Laser by optical Feedback for Stontium BEC Applications*, B. Huang (master-thesis), University Innsbruck, Austria (2009).

[31] *FALC110 - Fast Analog Linewidth Control Manual*, Toptica Photonics AG, (2011).

[32] *Spherical Reference Cavities for Frequency Stabilization of Lasers in non-laboratory Environments*, D. R. Leibrandt, M. J. Thorpe, M. Notcutt, R. E. Drullinger, T. Rosenband, and J. C. Bergquist, Opt. Express **19**, 3471 (2011).

[33] *Thermal-noise Limit in the Frequency Stabilization of Lasers with Rigid Cavities*, K. Numata, A. Kemery, and J. Camp, Phys. Rev. Lett. **93** (2004).

[34] *Overview over the Control System of the Strontium experiment*, F. Schreck, URL: http://iqoqi.at/control (2012).

[35] *Impedance Matching for High-Frequency Circuit Design*, M. Tse, URL: http://cktse.eie.polyu.edu.hk/eie403/impedancematching.pdf (2003).

[36] *Negative-Stiffness Vibration Isolators – How they Work*, M.-K. Technology, URL: http://www.minusk.com (2012).

[37] *BM-4 Bench Top Vibration Isolation Platform*, Minus-K Technology, URL: http://www.minusk.com .

[38] *Introduction to Quantum Mechanics*, D. J. Griffiths (Pearson Prentice Hall, 2005).

[39] *Colloquium : Physics of Optical Lattice Clocks*, A. Derevianko and H. Katori, Rev. Mod. Phys. **83**, 331 (2011).

[40] *Sideband Cooling while Preserving Coherences in the Nuclear Spin State in Group-II-like Atoms*, I. Reichenbach and I. H. Deutsch, Phys. Rev. Lett. **99**, 123001 (2007).

[41] *State-dependent, Addressable Subwavelength Lattices with Cold Atoms*, W. Yi, A. J. Daley, G. Pupillo, and P. Zoller, New J. Phys. **10**, 073015 (2008).

[42] *Two-orbital SU(N) Magnetism with Ultracold Alkaline-Earth Atoms*, A. V. Gorshkov, M. Hermele, V. Gurarie, C. Xu, P. S. Julienne, J. Ye, P. Zoller, E. Demler, M. D. Lukin, and A. M. Rey, Nature Phys. **6**, 289 (2010).

[43] *High Precision Spectroscopy of Strontium in an Optical Lattice: Towards a New Standard for Frequency and Time*, M. Boyd (PHD-thesis) (University of Colorado, 2002).

Danksagung

An vorderster Stelle möchte ich mich bei dem ganzen Strontium Team bedanken. Ohne euch wären die letzten Monate nicht möglich gewesen.

Ich danke Florian, der mich herzlich in seine Gruppe aufgenommen hat und jederzeit ein offenes Ohr für all meine Anliegen hatte. Florian war jederzeit für mich da und hat mich unterstützt – mit Hilfestellung bezüglich Laborarbeit, Diskussion über physikalische Themen, Einführung in die wissenschaftliche Welt oder Ratschlag bezüglich einer wissenschaftliche Zukunft – selbst wenn er selbst mit Arbeit eingedeckt war. Vielen Dank für das letzte Jahr.

Ich bedanke mich bei Simon und Benjamin für die viele Hilfe an meinem Projekt und die experimentellen Tipps die sie mir gegeben haben und welche sonst schwer zu bekommen sind. Wenn es mal Kritik gab, dann war sie offen und ehrlich, und hat mich wachsen lassen. Danke auch dafür.

Vielen herzlichen Dank auch an Alex und Slava, dafür dass sie immer für Diskussionen bereitstanden und mich mit guten Ideen oft weiterbrachten.

An dieser Stelle möchte ich mich auch besonders bei Simon, Florian und Benjamin dafür bedanken, dass sie einiges ihrer Lebenserfahrung und Weisheit mit mir geteilt haben. Das letzte Jahr war nicht nur eine wissenschaftliche Reise für mich, sondern auch ein persönliches. Eine Reise in der ich viel über mich selbst und meine Zukunft von euch lernen konnte.

Ich bedanke mich bei Rudi Grimm, dafür dass ich in seiner Gruppe mitarbeiten durfte, welche Wissenschaft auf höchstem Niveau und angenehmes Arbeitsklima verbindet. Außerdem danke ich ihm dafür, dass seine Ansätze und Ideologien mir immer ein Vorbild waren.

Ohne die tatkräftige Mithilfe vieler Leute am IQOQI wäre das Projekt natürlich nur schwerlich möglich gewesen. Stellvertretend für die Mitarbeiter des IQOQIs möchte ich mich besonders bei Stefan und Andreas in der mechanischen Werkstatt bedanken, welche mir alles über Metallverarbeitung beigebracht haben, was ich weiß. Drehen und Fräsen zu lernen hat mir besondere Freude bereitet. Auch bei Gerhard möchte ich mich bedanken, dass er bei allen elektronischen und technischen Fragen sofort zur Stelle war und vor allem für seine lebensrettende Hilfe im Fall des EOMs. Nur durch Doris und Elisabeth war die schnelle und unkomplizierte Art und Weise möglich mit der Bestellungen und andere Rahmenarbeiten zum Projekt erledigt werden konnten. Auch vielen Dank für die Geduld im Fall der Zollprobleme.

Bei Michael Chwalla aus dem Nachbarlabor möchte ich mich für die enge Zusammenarbeit bei unseren Laserprojekten bedanken und dafür, dass er mir viele Dinge über Laserphysik und Lasertechnik beigebracht hat.

Meinen Studienfreunden Simon, Christian und Mike möchte ich dafür danken, dass sie mich die letzten fünf Jahre begleitet haben. Ohne sie hätte

ich nicht halb so viel gelernt, nicht halb so viel verstanden und hätte nich halb so viel Spaß gehabt. Neben gemeinsamen Rechnen der Proseminar Aufgaben, Vorbereiten auf Prüfungen gab es auch einiges zu Lachen. Egal ob Simons berühmte rechte Hand Regel mit linker Hand, Mikes Lebensweisheit in Form von "Das brauch ich nicht – interessiert mich nicht." oder Christians "Ich hohl mal meine sechs Meter lange Tafel" – viele Situationen werden mir in Erinnerung bleiben.